

**Evaluation of the Classical Reaction Engineering models in
terms of mass transport and reaction rate distribution for
low tube-to-particle diameter ratio beds.**

by
M. Florent Allain

A dissertation submitted to the faculty of the
Worcester Polytechnic Institute
in partial fulfillment of the requirements
for the Degree of Master of Science
in Chemical Engineering

May 2011

Approved

Prof. A. G. Dixon, Advisor

Prof. D. DiBiasio, Department Head

Summary

Packed bed reactors are widely used in the chemicals industry and have been studied carefully in the last century. Several reaction engineering models have been developed in order to predict the behavior of such reactors under specified conditions, in order to assist in the sizing during an industrial process conception.

These reactors can be categorized using different parameters, and the bed-to-particle diameter ratio - N - is one of them. It has been shown that this parameter influences greatly the transfer phenomena that occur in the bed, and that for ratios under 10, particular attention is needed when considering the wall effects. An important point that has to be evaluated is the accuracy of the actual chemical reaction engineering models when simulating such beds as it is valid to question the hypothesis of a pseudo-continuum model when considering a low bed-to-particle diameter ratio bed.

Through high precision Computational Fluid Dynamics calculations, several beds of particles are modeled and studied in term of mass dispersion and reaction rate distribution. Two reaction engineering models - a simple pseudo-continuum model with effectiveness factor, and a model we refer to as "Single pellet" model - and several correlations regarding Peclet numbers are then evaluated under the same conditions in order to determine their accuracy and reliability for that particular kind of bed.

Two beds of $N = 5.96$ and $N = 7.99$ are studied for dispersion phenomena, and the bed of $N = 5.96$ is studied for reaction rate distribution. It is shown that the pseudo-continuum model of dispersion stands valid for the higher N , but that none of the correlations we used were able to correctly predict the behavior of the $N = 5.96$ bed at any of the Reynolds number we considered, only giving close behaviors. We were confronted with some difficulties regarding the reaction simulation under Fluent, but some comparisons were successfully made regarding species and reaction rate distribution in the bed.

Acknowledgment

Time flies. And this is clearly something I experienced here in Worcester. 18 months ago I arrived with all the doubts that moving 5000 miles away from home can give you. I can now gladly say that I enjoyed every moment I spent here. Sure Worcester is not the greatest city in America, but I will regret leaving all the wonderful people I met there, who gave me the support I needed.

First, I would like to thank my advisor, Professor Dixon for his help, guidance and advices. I would not have been able to complete this work without his support, moral and financial. I wanted to thank him particularly for giving me the opportunity to speak about my work at the 2010 COMSOL conference in Boston. For all this and for more, thank you.

I also want to thank my roommates Jeff and Thomas, as well as Sarah, for all the support you gave me during these two years, and for making me feel at home here. Thank you also to Mohsen, for keeping me company in the lab.

Thank you to all the Chemical Engineering Department, for granting me a Teaching Assistantship for my second year. It confirmed my thoughts that I am probably not suited for a career in academics, but I am sure the things I learnt will come in handy some day.

Last but not least, I can never be grateful enough to my parents, Jean-Pierre and Josiane, and my sister Aurore, who supported me all these years. I would not be here today without their constant encouragements and advices.

Florent.

Contents

Summary	i
Acknowledgment	ii
I Introduction	10
1 Low-N packed bed reactors	10
2 Dispersion in packed beds	11
3 Reaction Engineering models	15
3.1 Pseudo-Homogeneous models	15
3.2 Pseudo-Heterogeneous models	16
3.3 The problem of low-N packed beds	21
II Computational Fluid Dynamic approach	23
1 Meshing	23
1.1 Dispersion	24
1.2 Dispersion with reaction inside the catalyst particles	26
2 Calculations	27
2.1 Dispersion	27
2.2 Dispersion with reaction inside the catalyst particles	29

III	Reaction Engineering approach	30
1	Convection-Diffusion simulations	30
2	Convection-Diffusion and reaction simulations	34
2.1	Pseudo-Heterogeneous model with effectiveness factor.	35
2.2	Single Pellet model	36
IV	Results and discussion	38
1	Dispersion model	38
1.1	Packed bed of $N = 5.96$	39
1.2	Packed bed of $N = 7.99$	49
1.3	Implementation of the velocity and porosity profiles $u(r)$ and $\epsilon(r)$. .	58
2	Reaction models	64
	Conclusion	73
	Recommendation	74
1	Dispersion calculations	74
2	Reaction calculations	74
	Nomenclature	75
	Appendices	81

A	Reaction Parameters	81
B	Values of axial and radial Peclet numbers for the different correlations	82
B.1	Foumeny et al.	82
B.2	Coelho et al.	82
B.3	Freud et al.	83

List of Figures

1	<i>Effectiveness factor as a function of the Thiele modulus. Case of a sphere.</i>	18
2	<i>Comparison of high and low N packed beds</i>	21
3	<i>Packed bed of $N = 7.99$, gaps configuration.</i>	24
4	<i>Boundary layers around a particle connected to the wall by a bridge, $N = 7.99$.</i>	25
5	<i>Geometry of the Fluent model. Source term pictured in red.</i>	28
6	<i>Build up of CH_4 between a particle and the wall, $N = 5.96$, gaps configuration.</i>	28
7	<i>Geometry of the Convection-Diffusion model in COMSOL.</i>	31
8	<i>First model for the source term in COMSOL.</i>	32
9	<i>Comparison between the Fluent and COMSOL geometries for Convection-Diffusion calculations.</i>	33
10	<i>Mesh of the COMSOL Convection-Diffusion, near the symmetry axis and source.</i>	34
11	<i>Geometry of the Singel Pellet model.</i>	36
12	<i>Iso-clips created on Fluent at $z=7''$ and $12''$ for $N = 7.99$.</i>	39
13	<i>Concentration profile of CH_4 at $z=5''$ for $N = 5.96$, $Re=87$, Gaps configuration.</i>	40
14	<i>Concentration profile of CH_4 at $z=5''$ for $N = 5.96$, $Re=87$, Bridges configuration.</i>	41
15	<i>Concentration profile of CH_4 at $z=10''$ for $N = 5.96$, $Re=87$, Gaps configuration.</i>	41
16	<i>Concentration profile of CH_4 at $z=10''$ for $N = 5.96$, $Re=87$, Bridges configuration.</i>	42
17	<i>Concentration profile of CH_4 at $z=5''$ for $N = 5.96$, $Re=348$, Gaps configuration.</i>	42

18	<i>Concentration profile of CH₄ at z=5" for N = 5.96, Re=348, Bridges configuration.</i>	43
19	<i>Concentration profile of CH₄ at z=10" for N = 5.96, Re=348, Gaps configuration.</i>	43
20	<i>Concentration profile of CH₄ at z=10" for N = 5.96, Re=348, Bridges configuration.</i>	44
21	<i>Concentration profile of CH₄ at z=5" for N = 5.96, Re=696, Gaps configuration.</i>	44
22	<i>Concentration profile of CH₄ at z=5" for N = 5.96, Re=696, Bridge configuration.</i>	45
23	<i>Concentration profile of CH₄ at z=10" for N = 5.96, Re=696, Gaps configuration.</i>	45
24	<i>Concentration profile of CH₄ at z=10" for N = 5.96, Re=696, Bridges configuration.</i>	46
25	<i>Concentration profile of CH₄ at z=5" for N = 5.96, Re=870, Gaps configuration.</i>	46
26	<i>Concentration profile of CH₄ at z=5" for N = 5.96, Re=870, Bridges configuration.</i>	47
27	<i>Concentration profile of CH₄ at z=10" for N = 5.96, Re=870, Gaps configuration.</i>	47
28	<i>Concentration profile of CH₄ at z=10" for N = 5.96, Re=870, Bridges onfiguration.</i>	48
29	<i>Concentration profile of CH₄ at z=7" for N = 7.99, Re=87, Gaps configuration.</i>	50
30	<i>Concentration profile of CH₄ at z=7" for N = 7.99, Re=87, Bridges configuration.</i>	50
31	<i>Concentration profile of CH₄ at z=12" for N = 7.99, Re=87, Gaps configuration.</i>	51
32	<i>Concentration profile of CH₄ at z=12" for N = 7.99, Re=87, Bridges configuration.</i>	51

33	<i>Concentration profile of CH₄ at z=7" for N = 7.99, Re=348, Gaps configuration.</i>	52
34	<i>Concentration profile of CH₄ at z=7" for N = 7.99, Re=348, Bridges configuration.</i>	52
35	<i>Concentration profile of CH₄ at z=12" for N = 7.99, Re=348, Gaps configuration.</i>	53
36	<i>Concentration profile of CH₄ at z=12" for N = 7.99, Re=348, Bridges configuration.</i>	53
37	<i>Concentration profile of CH₄ at z=7" for N = 7.99, Re=696, Gaps configuration.</i>	54
38	<i>Concentration profile of CH₄ at z=7" for N = 7.99, Re=696, Bridges configuration.</i>	54
39	<i>Concentration profile of CH₄ at z=12" for N = 7.99, Re=696, Gaps configuration.</i>	55
40	<i>Concentration profile of CH₄ at z=12" for N = 7.99, Re=696, Bridges configuration.</i>	55
41	<i>Concentration profile of CH₄ at z=7" for N = 7.99, Re=870, Gaps configuration.</i>	56
42	<i>Concentration profile of CH₄ at z=7" for N = 7.99, Re=870, Bridges configuration.</i>	56
43	<i>Concentration profile of CH₄ at z=12" for N = 7.99, Re=870, Gaps configuration.</i>	57
44	<i>Concentration profile of CH₄ at z=12" for N = 7.99, Re=870, Bridges configuration.</i>	57
45	<i>Porosity profile for N = 5.96. Red: Bridges, Blue: Gaps</i>	58
46	<i>Porosity profile for N = 7.99. Red: Bridges, Blue: Gaps</i>	59
47	<i>Mean velocity profile for N = 5.96, Re = 348, Red: Bridges, Blue: Gaps</i>	60
48	<i>Concentration profiles for N = 5.96, Re = 348, correlation by Foumeny et al. at z'=5</i>	60

49	<i>Concentration profiles for $N = 5.96$, $Re = 348$, correlation by Foumeny et al. at $z'=10$</i>	61
50	<i>Concentration profiles for $N = 5.96$, $Re = 348$, correlation by Coelho et al. at $z'=5$</i>	61
51	<i>Concentration profiles for $N = 5.96$, $Re = 348$, correlation by Coelho et al. at $z'=10$</i>	62
52	<i>Concentration profiles for $N = 5.96$, $Re = 348$, correlation by Freund et al. at $z'=5$</i>	62
53	<i>Concentration profiles for $N = 5.96$, $Re = 348$, correlation by Freund et al. at $z'=10$</i>	63
54	<i>Peclet numbers obtained in COMSOL for $N = 5.96$, $Re = 348$, gaps configuration, with porosity and interstitial velocity profiles</i>	64
55	<i>Concentration profile of CH_4 at $z=7''$ and $12''$, Pseudo-heterogeneous model.</i>	67
56	<i>Concentration profile of H_2 at $z=7''$ and $12''$, Pseudo-heterogeneous model.</i>	68
57	<i>Concentration profile of CO at $z=7''$ and $12''$, Pseudo-heterogeneous model.</i>	68
58	<i>Concentration profile of H_2O at $z=7''$ and $12''$, Pseudo-heterogeneous model.</i>	69
59	<i>Concentration profile of CH_4 at $z=7''$ and $12''$, Single pellet model.</i>	70
60	<i>Concentration profile of H_2 at $z=7''$ and $12''$, Single pellet model.</i>	70
61	<i>Concentration profile of CO at $z=7''$ and $12''$, Single pellet model.</i>	71
62	<i>Concentration profile of H_2O at $z=7''$ and $12''$, Single pellet model.</i>	71

List of Tables

1	<i>Percentage of particles in contact with the wall for different N</i>	11
2	<i>Example of values of N for which Pe_a reaches very low values</i>	12
3	<i>Mesh parameters for the $N = 5.96$ bed, all Reynolds numbers, before adaptations.</i>	25
4	<i>Mesh parameters for the $N = 7.99$ bed, all Reynolds numbers.</i>	26
5	<i>Mesh parameters for the $N = 5.96$ bed with reaction.</i>	27
6	<i>Subdomain settings and Boundary settings as entered in COMSOL for the Convection-Diffusion model computations</i>	31
7	<i>Source term concentration C_0 in mol.m^{-3} for each COMSOL file</i>	33
8	<i>Comparison between outlet fluxes (in $\text{g.m}^{-2}.\text{s}^{-1}$ for two meshes, Pseudo-heterogeneous model.</i>	36
9	<i>Outlet fluxes (in $\text{g.m}^{-2}.\text{s}^{-1}$) of CH_4 for Fluent and COMSOL for $N=5.96$</i>	39
10	<i>Outlet fluxes (in $\text{g.m}^{-2}.\text{s}^{-1}$) of CH_4 for Fluent and COMSOL for $N=7.99$</i>	49
11	<i>Comparison between net fluxes and consumption/production/transfer term in COMSOL. Dimensionless.</i>	65
12	<i>Reaction rate and particle surface fluxes in COMSOL Single pellet model. Dimensionless.</i>	66
13	<i>Corrected solid surface flux and fluid transfer term.</i>	66
14	<i>Outlet fluxes (in $\text{g.m}^{-2}.\text{s}^{-1}$) for both models</i>	66
16	<i>Values of the constants required for the calculation of the reaction rate</i>	81
17	<i>Values of Peclet numbers calculated with the correlation from Foumeny et al.</i>	82
18	<i>Values of Peclet numbers calculated with the correlation from Coelho et al.</i>	82

19	Values of Peclet numbers calculated with the correlation from Freund et al.	83
----	--	----

Part I

Introduction

1 Low-N packed bed reactors

Being the simplest way to carry out a reaction on a catalyst, the packed bed reactor technology holds an important part of the chemical industry. Most of the actual chemical processes utilize a declination of a packed bed (reactors, gas/solid absorption...) at some stage of the production.

Among the ways of characterizing these reactors, one of the most important is the ratio between the bed and the catalyst particles diameter, N , which simply illustrate the number of particles that will fit on the diameter of the bed.

Most of the processes will use a bed with a high ratio ($12 < N < 500$) in which case the behavior throughout the bed will not be affected by any wall effect that could occur. These reactors will generally lead to a relatively uniform distribution of species, temperature and reaction rates, and only a restricted area will be affected by the wall effects.

Low N ratio beds ($N < 12$) present a good advantage for highly exo or endothermic reactions. When arranged in multi tubular reactors, these particular packed beds will ensure an improved heat exchange compared to their high N counterpart. However, when considering a low aspect ratio packed bed, one must be aware of the specific behavior regarding the transport phenomena across the bed. This kind of reactors will behave differently than high ratio packed beds, mainly because of wall effects, which do not limit themselves to a small region anymore. Indeed, these effects can extend to a distance equivalent to several particles away from the wall, which, in a reactor consisting of 6 particles along the bed diameter, will definitely have a serious impact. Studies that focused on the particles near the wall have shown that, the lower the N , the higher the percentage of particles that are going to be in contact with the wall of the reactor [17]. An example based on spherical particles is given in Table 1. These particles will behave differently than other particles, and show high gradients and asymmetric distributions of temperature, concentration and reaction rate.

N	% particles at the wall
4	69%
6	49%
8	38%
10	30%

Table 1: *Percentage of particles in contact with the wall for different N*

Moreover, when lowering the ratio to less than 4, it has been shown that the velocity profiles are severely modified, and a clear high velocity zone appears around the center of the bed [7].

These effects have been both observed in Computational Fluid Dynamic and experimental studies.

A big concern when looking at this kind of bed, is the lack of precision of the classical Reaction Engineering models, which we are going to discuss later on. We will also expose the problems one can encounter when simulating a low aspect ratio bed with these models.

2 Dispersion in packed beds

The phenomenon of dispersion in beds of packed particles has been intensively studied for both organized and random packing of particles of different shapes. A large number of studies have been conducted both experimentally and through Computational Fluid Dynamics calculations [3–6, 9, 10, 12, 13, 16, 21, 23–25].

When discussing the subject of dispersion, one can define the Peclet number based on the catalyst particle diameter:

$$Pe_m = \frac{u_o d_p}{\mathcal{D}_m}$$

with u_o being the superficial velocity, d_p the catalyst particle diameter and \mathcal{D}_m the molecular diffusivity of the considered species.

The dispersion phenomenon can be divided in two distinct components when considering an axial symmetric bed: the radial component Pe_r and the axial one Pe_a , respectively defined using the radial and the axial component of the effective

diffusivity. This dispersion is the principal mechanism of mass transport in packed beds, and also influences the heat transfer.

It has been shown that radial and axial Peclet number are depending on the molecular Peclet number Pe_m , which is the product of the Schmidt and the Reynolds numbers. When considering regular packed beds, with high N , it has been observed that for high Reynolds, the Peclet numbers are going to reach an asymptotic value, observed to be around 12 for the radial component, and 2 for the axial one. Correlations have been established for these two numbers [6]:

$$\frac{1}{Pe_a} = \frac{1}{\tau Pe_m} + \frac{1}{2} \quad (1)$$

$$\frac{1}{Pe_r} = \frac{1}{\tau Pe_m} + \frac{1}{12} \quad (2)$$

However, the values of the Peclet numbers depend on a lot of parameters, including the ratio between column length and diameter, particle shape and size distribution, and also on the ratio between bed and particle diameter.

As a result, when considering the case of low N packed beds, the classical asymptotic values of 2 and 12 are no longer valid. Indeed, there have been claims of bigger axial dispersion for beds of N between 1.9 and 4.7. However, between $N = 1.1$ and $N = 1.4$, the dispersion do not seem to be any higher than for $N > 15$ [1, 22]. Table 2 shows some values of the axial Peclet number for very low N [1].

N	ϵ	$Pe_{m,a}$
4.7	0.676	0.14
3.5	0.692	0.18
1.9	0.709	1.00

Table 2: *Example of values of N for which Pe_a reaches very low values*

Fahien and Smith [8] were among the first to introduce a correlation for the radial Peclet number that involved the ratio between bed and particle diameters:

$$Pe_{m,r} = \frac{u_o d_p}{D_r} \frac{1}{1 + 19(d_p/d_t)^2} \quad (3)$$

Foumeny et al. later proposed correlations based on experimentations run at low

N (3.2, 4.2, 7.3, 8.6) [9]. Their paper was aimed at developing a two dimensional model implementing both axial and radial dispersion. When running the experiment, measurements were made at 3 different axial positions in the bed, 4 radial positions, and at 8 different angles. Both transient and steady state behavior were studied. They worked over a wide range of particle Reynolds number (0.3 to 806), as well as a wide range of aspect ratio N (3.2 to 25.3). As a conclusion to their study, they suggested the following correlations for axial and radial Peclet numbers at steady state:

$$\frac{1}{Pe_{m,r}} = \frac{0.34}{(Re_0Sc)^{0.80}} + \frac{0.08}{\left(1 + \frac{10.8}{Re_0Sc}\right)} \quad (4)$$

$$\frac{1}{Pe_{m,a}} = \frac{0.72}{ReSc} + \frac{0.52}{\left(1 + \frac{9.0}{ReSc}\right)} \quad (5)$$

These correlations depend directly on the Reynolds and Schmidt number (or the molecular Peclet number Pe_m). However, there is no direct relation with the bed-to-particle diameter ratio.

Magnico [16] obtained values for the Peclet numbers for different bed-to-particle diameter ratios. CFD simulations of dispersion in bed of $N=5.96$ and 7.3 were run using Lagrangian and Eulerian methods, for Reynolds from 7 to 200. The packed beds were obtained using the Bennet method, with gravity stability condition. A sphere is added to a random position on a horizontal plane, and to guarantee stability, this sphere must be in contact with three other particles. The Navier-Stokes equations were solved using a finite volume method with structured mesh. Axial Peclet numbers of respectively 1.075 and 1 were obtained, as well as a ratio of D_a/D_r of 7 and 5, which would lead to radial Peclet numbers of 7.527 and 5. According to the author, these values are independent of the Reynolds number.

Freund et al. [10] established correlations for axial and radial dispersion coefficient using the lattice Boltzmann method on structured and random packing of spherical particles with $N=5$, and for Peclet number between 0.3 and 187 for the random packing. This packing was obtained with a Monte-Carlo based method, imitating the real life filling process of a column, making particles rain in a cylindrical tube, and then rearranging the spheres accordingly with gravity. Their simulation was based on the lattice-Boltzmann method, namely the D3Q19 model, using a MAC approach for the no-slip boundary conditions at the solid-wall interfaces. The mass

transport was studied using the Particle tracking method. The correlations they propose for the random packing are the following:

$$\frac{D_{rad}}{\mathcal{D}_m} = \frac{1}{\tau} + \frac{Pe_m^{\alpha_{rad}}}{\beta_{rad}} \quad (6)$$

$$\frac{D_{ax}}{\mathcal{D}_m} = \frac{1}{\tau} + a_1 Pe_m + a_2 Pe_m \ln(Pe_m) \quad (7)$$

with $\tau = 1.45$, $\alpha_{rad} = 0.85$, $\beta_{rad} = 10$, $a_1 = 0.005$ and $a_2 = 0.177$. Axial dispersion, at first, was correlated the same way as the radial one, but a logarithmic model was latter adopted since it seemed to fit their data better.

Coelho et al. [4] focused on transport properties in beds with random packing of ellipsoid particles. Their random packing was generated using a "free fall method", and the grains fall from a random location until they attain a minimum in their potential energy. The detailed algorithm is described by Coelho et al. in their paper. They studied not only mass transfer parameters but also several geometrical properties of the beds, like the porosity, specific surface area, and grain ordering. Thermal conduction was solved with a second order finite-difference formulation. Stokes flow was solved with a fourth order finite-difference scheme. For dispersion, a conjugate-gradient iterative scheme was used. For spherical particles in a packed bed of $N=7.5$, and for Peclet number between 10 and 2000, they developed the following correlations:

$$\frac{D_{rad}}{\mathcal{D}_m} = 0.164 Pe_m^{0.72} \quad (8)$$

$$\frac{D_{ax}}{\mathcal{D}_m} = 0.106 Pe_m^{1.29} \quad (9)$$

These correlations would also be applicable for ellipsoidal particles.

The last three sets of correlation, by Freund et al., Coelho et al. and Foumeny et al., as well as the Reynolds independent values found by Magnico were retained for our study and the comparison between reaction engineering models and CFD calculations.

3 Reaction Engineering models

Reaction engineering models are based on a pseudo-continuum assumption. This assumption relies on the fact that a particle diameter is very small when compared to the bed diameter, making the bed uniform. This leads to the fact that at every point of the model, there is both solid and fluid, with the reaction rate based on the solid temperature and concentrations. These models are then separated in two categories, the Pseudo-Homogeneous and Pseudo-Heterogeneous models, which are described in the next sections.

All the equations presented here are based on a reaction of the form $\sum_{i=1}^n \nu_i A_i = 0$ with ν_i positive for a product, with a reaction rate of $R(C_i, T)$.

We will here expose briefly different models, as this has been done before in the literature [11].

3.1 Pseudo-Homogeneous models

The first type of Reaction Engineering models, and the simplest one considering convection and diffusion, are the Pseudo-Homogeneous models. The first assumption that is done in these models, is the fact that both fluid and solid are at the same temperature and concentrations. Therefore, for a system of n species, there only are $n+1$ equations - one for each species and one for the temperature - which simplifies greatly the calculations. Equations 10 and 11 are the dimensionless steady-state equations used in this model, when considering constant radial and axial diffusivity.

$$\frac{-\partial C'_i}{\partial z'} + \frac{1}{Pe_{m,r,i}} \left(\frac{\partial^2 C'_i}{\partial r'^2} + \frac{1}{r'} \frac{\partial C'_i}{\partial r'} \right) + \frac{1}{Pe_{m,a,i}} \frac{\partial^2 C'_i}{\partial z'^2} = -\nu_i (1 - \epsilon) Da \mathcal{R}(C'_i, T') \quad (10)$$

$$-\frac{\partial T'}{\partial z'} + \frac{1}{Pe_{h,r,i}} \left(\frac{\partial^2 T'}{\partial r'^2} + \frac{1}{r'} \frac{\partial T'}{\partial r'} \right) + \frac{1}{Pe_{h,a,i}} \frac{\partial^2 T'}{\partial z'^2} = (1 - \epsilon) \beta_f Da \mathcal{R}(C'_i, T') \quad (11)$$

where $C'_i = C_i/C_{tot}$, $T' = T/T_{in}$, $r' = r/d_p$, $z' = z/d_p$, Da is the Damkhöler number and β_f the adiabatic temperature rise of the fluid. i goes from 1 to n , for each species.

The equations are coupled with the following boundary conditions.

$$\begin{aligned}
 r' = 0 \quad \frac{\partial C'_i}{\partial r'} = 0, \quad \frac{\partial T'}{\partial r'} = 0 \\
 r' = R_t/d_p \quad \frac{\partial C'_i}{\partial r'} = 0, \quad \frac{\partial T'}{\partial r'} = Bi_w(T'_w - T') \\
 z' = 0 \quad \frac{\partial C'_i}{\partial z'} = Pe_{m,a}(C'_i - C'_{i,in}), \quad \frac{\partial T'}{\partial z'} = Pe_{h,a}(T' - T'_{in}) \\
 z' = L/d_p \quad \text{convective fluxes}
 \end{aligned}$$

As we already said before, this model leads to simple computations, and will only be suitable for steady states with simple systems. One has to carefully select the heat and mass transfer parameters, and be cautious when selecting the bulk temperature. Indeed if the ΔT between the two phases reaches a high value experimentally, this model will not be suitable. Another drawback of these Pseudo-Homogeneous equations is that they do not take into account the diffusion in the particles of catalyst, assuming an instant diffusion, and no reaction limitation. This problem can be solved by adding an effectiveness factor to these equations. The effectiveness factor will be discussed in the next section.

This Pseudo-Homogeneous model can be simplified even further by assuming the predominance of radial or axial mixing, or by even totally neglecting the convection phenomena, but we will not cover these simplifications here.

3.2 Pseudo-Heterogeneous models

When considering solid and fluid as two different phases, with different concentrations and temperatures, one moves to Pseudo-Heterogeneous models. In these models, the solid provides the source terms at each and every point of the bed, modeled as being entirely filled by the fluid phase. This introduces the transfer limitations between solid and fluid and therefore reflects the differences in temperatures and concentrations.

These models consist of 2 convection-conduction equations for the temperature and $2.n$ convection-diffusion equations for the n components of the system. The simplest of these Pseudo-Heterogeneous model is represented by Equations 12 - 15 and their boundary conditions. Both axial and radial diffusivities are considered

constant.

Fluid phase:

$$-\frac{\partial C'_{f,i}}{\partial z'} + \frac{1}{Pe_{m,r,i}} \left(\frac{\partial^2 C'_{f,i}}{\partial r'^2} + \frac{1}{r'} \frac{\partial C'_{f,i}}{\partial r'} \right) + \frac{1}{Pe_{m,a,i}} \frac{\partial^2 C'_{f,i}}{\partial z'^2} = St_{m,i}(C'_{f,i} - C'_{s,i}) \quad (12)$$

$$-\frac{\partial T'_f}{\partial z'} + \frac{1}{Pe_{h,r,i}} \left(\frac{\partial^2 T'_f}{\partial r'^2} + \frac{1}{r'} \frac{\partial T'_f}{\partial r'} \right) + \frac{1}{Pe_{h,a,i}} \frac{\partial^2 T'_f}{\partial z'^2} = St_h(T'_f - T'_s) \quad (13)$$

Solid phase:

$$St_{m,i}(C'_{f,i} - C'_{s,i}) = -\nu_i(1 - \epsilon)Da\mathcal{R}(C'_{s,i}, T'_s) \quad (14)$$

$$St_h(T'_f - T'_s) = (1 - \epsilon)\beta_f Da\mathcal{R}(C'_{s,i}, T'_s) \quad (15)$$

with the following boundary conditions:

$$r' = 0 \quad \frac{\partial C'_{f,i}}{\partial r'} = \frac{\partial C'_{s,i}}{\partial r'} = 0, \quad \frac{\partial T'_f}{\partial r'} = \frac{\partial T'_s}{\partial r'} = 0$$

$$r' = R_t/d_p \quad \frac{\partial C'_{f,i}}{\partial r'} = \frac{\partial C'_{s,i}}{\partial r'} = 0, \quad \frac{\partial T'_f}{\partial r'} = Bi_{f,w}(T'_w - T'_f), \quad \frac{\partial T'_s}{\partial r'} = Bi_{s,w}(T'_w - T'_s)$$

$$z' = 0 \quad \frac{\partial C'_i}{\partial z'} = Pe_{m,a}(C'_i - C'_{i,in}), \quad \frac{\partial T'_f}{\partial z'} = Pe_{h,a}(T'_f - T'_{in})$$

$$z' = L/d_p \quad \text{convective fluxes for the fluid, } \frac{\partial C'_{s,i}}{\partial z'} = 0, \quad \frac{\partial T'_s}{\partial z'} = 0$$

When compared to the Pseudo-Homogeneous model, this one introduces the effect of transfers between the two phases, but still assumes that the limiting phenomenon is the reaction inside the pellets, by not taking into account the diffusion. This problem can be addressed, again, via the introduction of an effectiveness factor η_i .

The effectiveness factor for species i can be defined as

$$\eta_i = \frac{\text{rate of reaction under diffusion limitation}}{\text{rate of reaction without diffusion resistance}}$$

It is related to the Thiele modulus Φ_i , defined as

$$\begin{aligned}\Phi_i^2 &= \frac{\text{reaction rate at uniform concentration } C_{s,i}}{\text{diffusion rate under concentration gradient } C_{s,i}/d_p} \\ &= \frac{d_p \rho_s R(C_{s,i}, T)}{D_{e,i} C_{s,i}/d_p}\end{aligned}$$

η_i and Φ_i^2 can be linked through a mathematical formula depending on the geometry of the catalyst particles. In the case of spherical isothermal particles like the one we will later consider for our calculations, the relation is the following:

$$\eta_i = \frac{3}{\Phi_i^2} (\Phi_i \coth(\Phi_i) - 1) \quad (16)$$

This function is plotted on Figure 1. When Φ_i is largely smaller than one, the effectiveness factor η_i tends toward 1 which means that diffusion is faster than the reaction, and when Φ_i becomes large, η_i falls asymptotic to $3/\Phi_i$ as the reaction becomes faster than the diffusion.

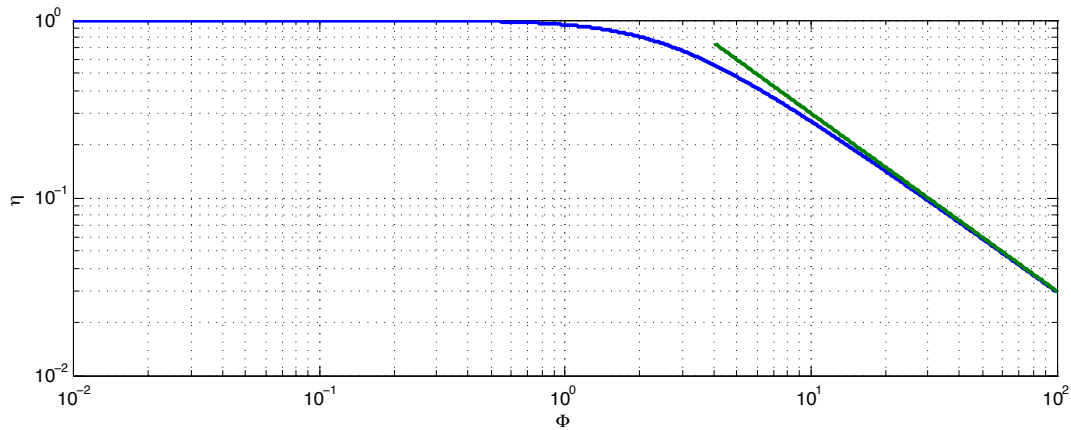


Figure 1: *Effectiveness factor as a function of the Thiele modulus. Case of a sphere.*

The implementation of η_i in Equations 14 and 15 adds to the model the effect of diffusion or reaction limitation in the solid. This leads to Equations 17 and 18, which share the same boundary conditions as Equations 14 and 15. The fluid equations are unchanged between the two models.

$$St_{m,i}(C'_{f,i} - C'_{s,i}) = -\nu_i(1 - \epsilon)\eta_i(\Phi_i)Da\mathcal{R}(C'_{s,i}, T'_s) \quad (17)$$

$$St_h(T'_f - T'_s) = (1 - \epsilon)\beta_f\eta_i(\Phi_i)Da\mathcal{R}(C'_{s,i}, T'_s) \quad (18)$$

The introduction of the effectiveness factor makes the model take diffusion limitations in the catalyst particles into account.

This model can be improved with the addition of thermal conduction in the solid bed, as energy is conducted through the contact points between the particles. The fluid equations stay unchanged, and as for the solid, only the thermal equation is modified as follow:

$$St_h(T'_f - T'_s) = (1 - \epsilon)\beta_f\eta_i(\Phi_i)Da\mathcal{R}(C'_{s,i}, T'_s) + \frac{1}{Pe_{h_{r,p}}} \left(\frac{\partial^2 T'_s}{\partial r'^2} + \frac{1}{r'} \frac{\partial T'_s}{\partial r'} \right) + \frac{1}{Pe_{h_{a,p}}} \frac{\partial^2 T'_s}{\partial z'^2} \quad (19)$$

This would take into account the possible conduction that would occur at the contact points between the particles of catalyst.

Finally, the last model considered here requires more computer power to be solved, which explains its lack of usage in the past. In this model - that we will now on refer to as the Single pellet model - the diffusion equations of mass and temperature inside the pellets of catalyst, are solved at every point of the bed. These equations are based on a Fick's law diffusion equation with constant intra-particle diffusivity. They also rely on the hypothesis of spherical particles surrounded by the uniform temperature and concentrations of the fluid at that particular point. This assumption of uniform surroundings comes from pseudo-continuum model hypothesis.

Solving these diffusion equations replaces the use of a global effectiveness factor. The fluid equations are almost unchanged, the only difference from Equations 12 and 13 being that the exchange terms between phases now consider the pellet surface temperature and concentrations, T_s^s and $C_{s,i}^s$.

The equations ruling this model are given below:

Fluid phase:

$$-\frac{\partial C'_{f,i}}{\partial z'} + \frac{1}{Pe_{m_{r,i}}} \left(\frac{\partial^2 C'_{f,i}}{\partial r'^2} + \frac{1}{r'} \frac{\partial C'_{f,i}}{\partial r'} \right) + \frac{1}{Pe_{m_{a,i}}} \frac{\partial^2 C'_{f,i}}{\partial z'^2} = St_{m,i}(C'_{f,i} - C'_{s,i}) \quad (20)$$

$$-\frac{\partial T'_f}{\partial z'} + \frac{1}{Pe_{h_r,i}} \left(\frac{\partial^2 T'_f}{\partial r'^2} + \frac{1}{r'} \frac{\partial T'_f}{\partial r'} \right) + \frac{1}{Pe_{h_a,i}} \frac{\partial^2 T'_f}{\partial z'^2} = St_h(T'_f - T'_s) \quad (21)$$

Solid phase:

$$\frac{-d^2 C'_{s,i}}{d\xi'^2} = \frac{2}{\xi'} \frac{dC'_{s,i}}{d\xi'} - \nu_i \Phi_i^2 \mathcal{R}(C'_{s,i}, T'_s) \quad (22)$$

$$\frac{-d^2 T'_s}{d\xi'^2} = \frac{2}{\xi'} \frac{dT'_s}{d\xi'} + \Phi_i^2 \beta_{s,i} \mathcal{R}(C'_{s,i}, T'_s) \quad (23)$$

with the following boundary conditions:

For the bed:

$$\begin{aligned} r' = 0 \quad & \frac{\partial C'_{f,i}}{\partial r'} = \frac{\partial C'_{s,i}}{\partial r'} = 0, \quad \frac{\partial T'_f}{\partial r'} = \frac{\partial T'_s}{\partial r'} = 0 \\ r' = R_t/d_p \quad & \frac{\partial C'_{f,i}}{\partial r'} = \frac{\partial C'_{s,i}}{\partial r'} = 0, \quad \frac{\partial T'_f}{\partial r'} = Bi_{f,w}(T'_w - T'), \quad \frac{\partial T'_s}{\partial r'} = Bi_{s,w}(T'_w - T'_s) \\ z' = 0 \quad & \frac{\partial C'_i}{\partial z'} = Pe_{m,a}(C'_i - C'_{i,in}), \quad \frac{\partial T'}{\partial z'} = Pe_{h,a}(T' - T'_{in}) \\ z' = L/d_p \quad & \text{convective fluxes for the fluid, } \frac{\partial C'_{s,i}}{\partial z'} = 0, \quad \frac{\partial T'_s}{\partial z'} = 0 \end{aligned}$$

For the particles:

$$\begin{aligned} \xi = 0 \quad & \frac{dC'_{s,i}}{d\xi'} = 0, \quad \frac{dT'_s}{d\xi'} = 0 \\ \xi = 1/2 \quad & -\frac{dC'_{s,i}}{d\xi'} = Sh_i(C'_{s,i} - C'_{f,i}), \quad -\frac{dT'_s}{d\xi'} = Bi_s(T'_s - T'_f) \end{aligned}$$

When using these equations, the diffusion or reaction rate limitations in the catalyst pellets is computed at every point of the bed, improving the precision of the calculations, but increasing the computation cost. Also, one must be very careful when selecting the values for the Sherwood and the Biot numbers, which rule the transfer between the two phases.

We exposed in this section some of the classical reaction engineering models that are used for the design and study of packed bed reactors. However, these models

where developed for high- N packed beds, and we are now going to see why they might need improvement when applied to low- N beds.

3.3 The problem of low- N packed beds

All the model that have been presented in the previous sections are based on the assumption of a Pseudo-Continuum bed. This means that the particles are considered to be present at every point of the bed, in relation to their diameter, which is assumed to be very small in comparison to the one of the tube.

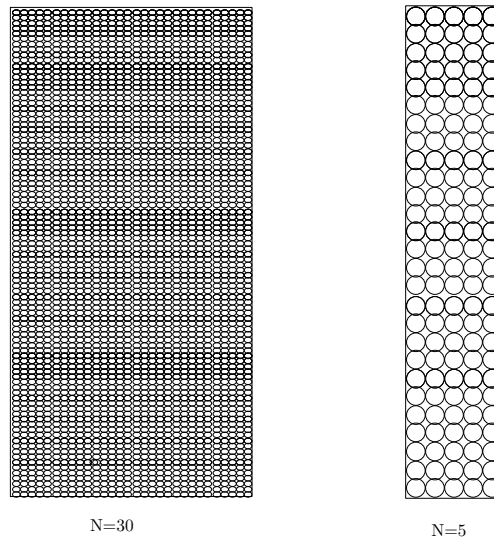


Figure 2: *Comparison of high and low N packed beds*

When looking at Figure 2, one can easily understand the problem of this assumption in the case of a low- N packed bed. And even though the figure illustrate the case of organized packing, the same observation can easily be pictured by the reader for randomized packed bed.

Assuming that both phases are present at every point of the bed is plausible when looking at a bed with $N=30$, but when only 5 particles can be found along the bed diameter, this assumption leads to a rough discretization of the bed, and the continuity hypothesis do not stand anymore.

This problem leads to some questioning about the possible use of porosity and velocity profiles along the bed radius instead of a mean porosity and velocity. Indeed, for high N beds, the porosity profiles are relatively flat and around the mean value, but when considering the high N beds, the porosity profiles present bigger variations. Moreover, the wall effects present the low- N beds are not properly reproduced with the classical models, mainly because of the use of this mean porosity. The question of using an axi-symmetrical model also rises some concerns as a randomly packed bed of low aspect ratio can easily lead to a non-symmetrical bed.

Moreover, the dispersion phenomena needs to be considered carefully as explained earlier in section I.1.

Part II

Computational Fluid Dynamic approach

1 Meshing

The evaluation of the dispersion in packed beds is relatively difficult experimentally, and Computational Fluid Dynamics provide us with tools to assess what would happen in a particular situation without having to run experiments. Moreover, it enables us to obtain data for the velocity field throughout the entire bed.

Two beds of different bed-to-particle diameter ratio were obtained, one of $N = 5.96$ and one of $N = 7.99$. These beds were obtained following two algorithms from the literature [18, 20]. The first layer of particles, at the bottom of the tube, is created using the method developed by Mueller. The base algorithm places spheres next to the wall of the bed, then moving towards the center. This algorithm was used specifically for the first layer, since the other one led to some problems. The rest of the bed is filled using the algorithm developed by Salvat et al. Both these algorithms are based on mono-sized particles. In the second part, gravitational field is accounted for, friction is neglected, spheres and wall are deformable and their contact forces are based on elasticity theory. The algorithm by Salvat et al. can be resumed as follows: A first stage where particles are randomly generated, allowing for overlaps. The second step consists in the implementation of the gravitational field in order to compact the bed, until the overlap between particles is acceptable.

Obtaining a good mesh in CFD is an extremely important part of the process. Two different meshes were created using Gambit for both $N = 5.96$ and $N = 7.99$ beds in order to evaluate their impact on the process of dispersion. Indeed, when modeling a full bed of particles, a decision has to be made regarding the way the contact points between particles and between the particles and the wall will be implemented. We chose two different approaches, both having been used previously in the literature [2, 15, 19]:

- The first one was to slightly reduce the diameter of the pellets to 99% of their original size, in order to leave a gap between every particle and between the particles and the wall. This will be referred to as the Gaps model.

- The second one was to create bridges between each particles where the contact point is supposed to happen. This will be referred to as the Bridges model.

A picture of the $N = 7.99$ bed with gaps configuration is given in Figure 3.

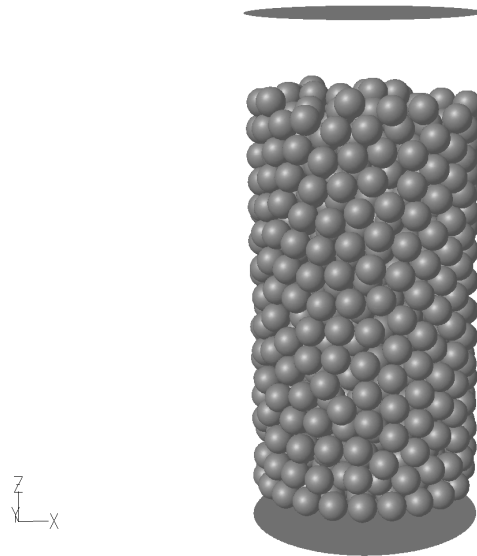


Figure 3: *Packed bed of $N = 7.99$, gaps configuration.*

Another possibility, that was not considered here, is to increase the diameter of the particles to 101% in order to have every particle overlap one another.

One problem that may arise from these geometries is that the gaps configuration underestimates the diffusion, by creating more pathways for the fluid between the particles and increasing the mean porosity of the bed. On the other hand, the bridges create more obstacles for the fluid, decreasing the porosity and increasing the dispersion.

The specific parameters of the mesh used for dispersion and reaction calculations are detailed next.

1.1 Dispersion

All the calculations run here were conducted using Fluent 6.3.26, the mesh being created on Gambit. All the calculations for dispersion in the bed of $N = 5.96$ were

ran on a Windows based server, with 2 Intel Xeon CPUs at 2.67GHz of RAM. Every other calculations were done on a 20 compute node Linux cluster (20 Intel P IV Xeon CPUs).

Calculations were run on the four different configurations: $N = 5.96$ with gaps and bridges, and $N = 7.99$ with gaps and bridges. The mesh statistics for the files with $N = 5.96$ and $N = 7.99$ are detailed in Table 3 and 4 respectively, for both gaps and bridges configurations. An example of the boundary layers for the bridges configuration is pictured in Figure 4.

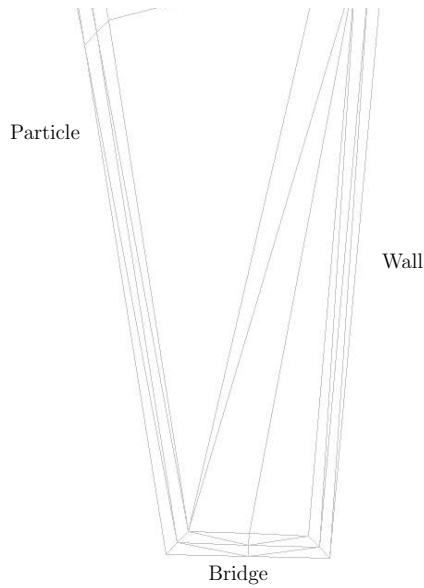


Figure 4: *Boundary layers around a particle connected to the wall by a bridge, $N = 7.99$.*

	Gaps model	Bridges model
Uniform mesh size	0.06"	0.06"
BL wall	3×0.001 "	2×0.001 "
BL particles	1×0.001 "	2×0.001 "
BL bridges	/	2×0.001 "
Tolerance for bridges generation	/	0.045"
Number of bridges	/	1411
Total number of cells	14.90M	13.75M
Number of cells in the source	2522	2522

Table 3: *Mesh parameters for the $N = 5.96$ bed, all Reynolds numbers, before adaptations.*

	Gaps model	Bridges model
Uniform mesh size	0.06"	0.06"
BL wall	3×0.001 "	2×0.001 "
BL particles	1×0.001 "	2×0.001 "
BL bridges	/	2×0.001 "
Tolerance for bridges generation	/	0.045"
Number of bridges	/	2943
Total number of cells	24.879M	25.13M
Highly skewed cells	1239	44
Number of cells in the source	2522	2522

Table 4: *Mesh parameters for the $N = 7.99$ bed, all Reynolds numbers.*

For both beds, in the gaps configuration the particles diameter is $d_p = 0.99$ ". Accordingly, the beds have a diameter of $d_t = 5.96$ " and $d_t = 8.00$ ". For the bridges configuration, the $N = 7.99$ bed has a particle diameter of $d_p = 0.9998$ " and a tube diameter of $d_t = 7.9902$ ". In order to establish the flow, an area of 1" is left empty before the bed, and 2" after. The length of the $N = 5.96$ files is 16.651" total, which makes the length of the bed 13.651". As for $N = 7.99$, the length of the bed is 14.712", with a total length of 17.712". In the case of $N = 5.96$, the bed consists of 400 particles, and 800 for $N = 7.99$.

1.2 Dispersion with reaction inside the catalyst particles

When considering reaction inside the catalyst particles, the gap model was retained. It seems fairly logical that the use of the bridge model would create direct communication between the particles, allowing for transfer from a particle to another. The bed being used in this case is the $N = 5.96$ bed, with the 400 particles of 0.99" diameter. The bed diameter was slightly increased to $d_t = 5.97$ ". The total length is 16.651", with the 1" and 2" empty zones before and after the bed. The first mesh parameters that were tested can be found in Table 5.

Later on, boundary layers were added inside the catalyst particles.

	Gaps model
Uniform mesh size	0.06"
BL wall	3×0.001 "
BL particles	1×0.001 "
Number of cells in each particle	17,000
Total number of cells	15.579M
Highly skewed cells	801

Table 5: *Mesh parameters for the $N = 5.96$ bed with reaction.*

2 Calculations

2.1 Dispersion

For the dispersion simulations, the calculations were run with a mixture of methane and air with a feed composed of pure air. Different inlet velocities were used: 0.05, 0.2, 0.4 and 0.5 m.s^{-1} . The regime was supposed laminar for the Fluent calculations. The source was implemented as follows.

We wanted the model to satisfy a simple mass balance: $F_{in} = F_{out}$, with no actual generation of matter, which would not have been the case with a classic source term. Moreover, when implementing an actual source in Fluent, it is considered solid, and therefore disrupts the velocity field around it, altering the diffusion and convection. These are the two principal reasons why the source term was implemented as a small cylinder of fluid, in which the mass fraction of CH_4 is set to 1. The cylinder, for both N , has a diameter of 0.05" and a length of 0.02". It is placed co-axially with the reactor, a few inches from the inlet of the bed (1.5" for the $N = 5.96$ case, 2" for $N = 7.99$) as pictured on Figure 5, in order to establish the velocity profile.

Conversion was assumed when dispersion was established and the residuals profiles were flat. In order to check for dispersion, the flow rate of CH_4 was calculated right after the source term, and at the outlet. The two values were then compared, and an error of 1% was considered acceptable.

In the case of $N = 5.96$, build-ups of methane were spotted between some particles and the wall, and mesh adaptations were conducted in order to limit these artifacts. This phenomenon can be seen on Figure 6. In order to minimize their influences in the final results, the mesh was adapted and refined where the concentration of methane was too high.

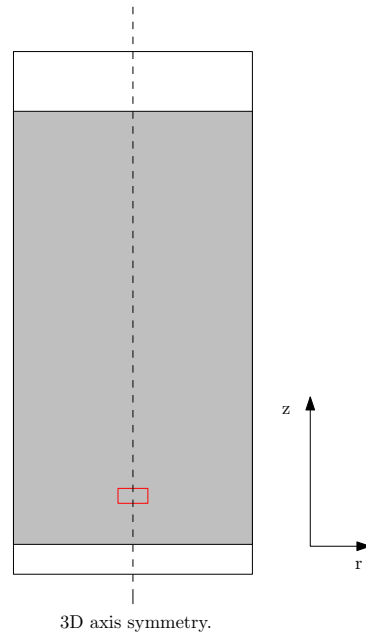


Figure 5: *Geometry of the Fluent model. Source term pictured in red.*

The grey area pictures the zone where particles are present.

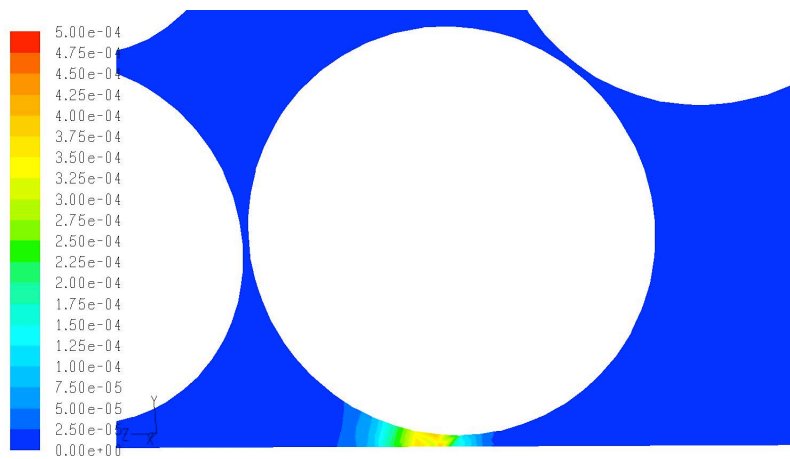


Figure 6: *Build up of CH_4 between a particle and the wall, $N = 5.96$, gaps configuration*

2.2 Dispersion with reaction inside the catalyst particles

The $N = 5.96$ bed was chosen to carry out the calculations including the reaction $CH_4 + H_2O \rightarrow CO + 3H_2$. The particles were meshed, and the reaction rate was implemented inside through the use of User Defined Functions. However, when considering the subject of dispersion into porous particles, Fluent can be unfriendly.

Previous calculations have shown that when using the models from Fluent, problem arose when looking at the solid surface velocity and fluxes between particles and fluid. When using these models, the velocity is set to 0 inside the particles, to account for the absence of convection in the pores. This setting causes Fluent to miscalculate the velocity at the interface between the two phases. Indeed, this velocity is calculated as an average between the fluid and the solid one, and therefore do not equal zero as it should.

This is why the use of User Defined Scalars in a plain solid particle is necessary. In that case, a zero velocity is automatically imposed at the interface, solving the previous problem. UDFs are then used to implement the diffusion and reaction inside the particles of catalyst.

The convergence was difficult and in order to make it easier, the reaction rate was modified. We started with several iterations with a reaction rate reduced by a factor of 1000. Then, after these iterations, more were conducted with a reaction rate divided by a factor 100. This was applied until the reaction rate was set to its real value, and then the calculations proceeded until convergence of the model.

This part discussed the implementation of our problem into Fluent, a CFD software. We will now discuss the implementation in COMSOL of the reaction engineering models.

Part III

Reaction Engineering approach

Models from Chemical Reaction Engineering were implemented using the COMSOL 3.5 Reaction Engineering module. Dimensionless equations were entered accordingly, First to simulate CH_4 diffusion in air through the two beds of particles of different aspect ratio, then adding the reaction $CH_4 + H_2O \rightarrow CO + 3H_2$, using the reaction rate proposed by Hou and Hughes [14] for the $N = 5.96$ bed. The models were implemented in different geometries accordingly to the phenomenon and aspect ratio that needed to be simulated.

1 Convection-Diffusion simulations

The first simulations to be run on COMSOL were to assess the accuracy of convection-diffusion models for low aspect ratio packed beds. The two beds introduced in Part II are considered.

The model we used was based on the convection-diffusion part of the models detailed previously. As we considered only one phase, fluid, flowing through a bed of particles, the choice of a specific model from Part I was not particularly important, as long as the convection, as well as the axial and radial diffusions, were included.

We used a steady state 2 dimensional axis-symmetric convection-diffusion model, following Equation 10, with the corresponding boundary conditions. The geometry is pictured in Figure 7. The source of CH_4 is pictured in red. Its implementation will be discussed later on.

In order to evaluate this model, we needed to obtain values for the axial and radial Peclet numbers. These values were computed through the use of the correlations from the literature that were discussed earlier. Equations 4-9 were therefore implemented in the COMSOL file. The model was also evaluated at Reynolds of 87, 348, 696 and 870. The molecular diffusivity \mathcal{D}_m for CH_4 was taken equal to $1.6 * 10^{-5} m^2 . s^{-1}$. The details for the *Subdomain settings* and *Boundary settings* in COMSOL are given in Table 6.(C0 being the concentration calculated for the source, as described later.)

One of the problems encountered during the modeling was the implementation of

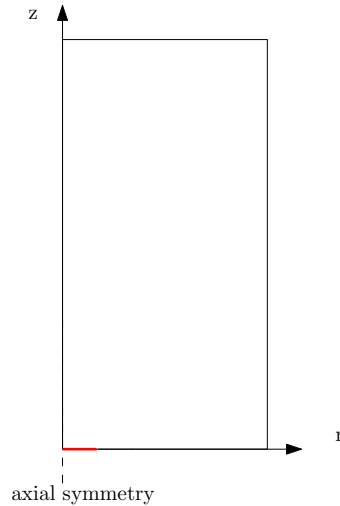


Figure 7: *Geometry of the Convection-Diffusion model in COMSOL.*

D (anisotropic)	1/Per 0 0 1/Pea
R	0
u	0
v	1
Left boundary	Insulation/Symmetry
Right boundary	Insulation/Symmetry
Inlet	$C_0=0$
Source (inlet)	$C_0=C_0$
Outlet	Convective flux

Table 6: *Subdomain settings and Boundary settings as entered in COMSOL for the Convection-Diffusion model computations*

a source term. The pre-defined source term function available in COMSOL was not adapted to our problem, as it results in a source present at one singular point of the geometry. The problem was that we wanted our source to be as close as possible as the one used in Fluent. Therefore, we first opted for adding half a square on the $r = 0$ axis at 1.5 inches from the inlet, with the same dimensions as in Fluent. Then through calculations based on the fluxes in each of the Fluent file, fluxes of CH_4 through the boundaries of this square were defined. This configuration is pictured

in Figure 8, with the source showed in red.

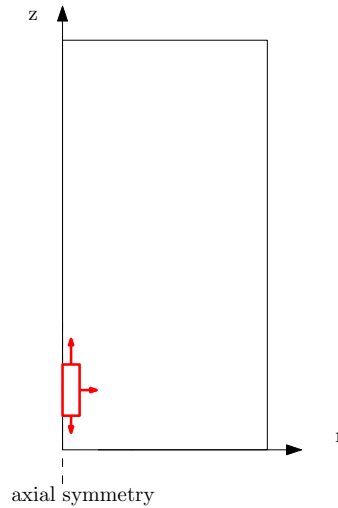


Figure 8: *First model for the source term in COMSOL.*

The problem with this method was that considering the low concentrations we were working with, the back mixing that is frequently observed with the classical convection-diffusion models was too important, and most of the CH_4 was diffusing against the flow. Accordingly we decided to create the source as a boundary, with a fixed concentration that was determined using the corresponding Fluent file. That boundary was placed at the inlet, and therefore the COMSOL simulation only covered the domain situated after the source in Fluent, as pictured in Figure 9.

All these calculations were run several times, based on the different configurations of the Fluent files as the gap and bridges configurations lead to differences in the porosity and velocity profiles, as well as in the concentration of the source term.

The value of the concentration C_0 for the source term was determined using the outlet mass flow rate of CH_4 in Fluent. This mass flow rate was then converted into a molecular flow rate and divided by the source outlet surface to get a flux and divided by the inlet velocity to obtain a concentration. Table 7 gives the value of this concentration for each file.

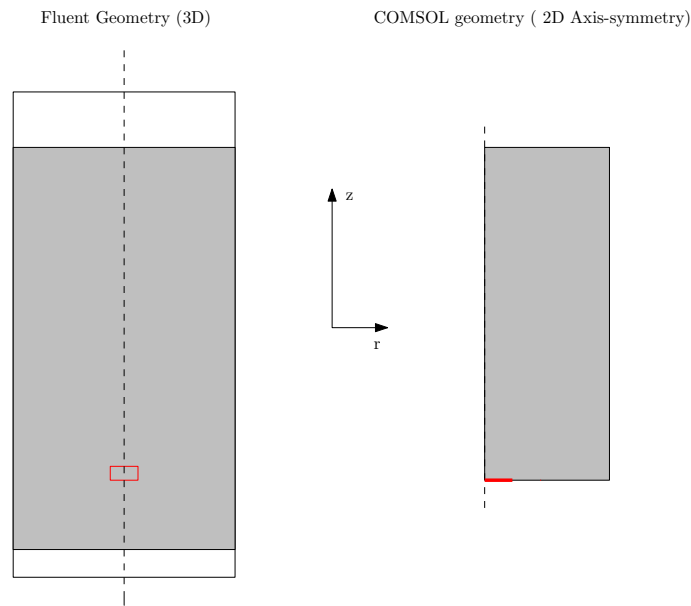


Figure 9: Comparison between the Fluent and COMSOL geometries for Convection-Diffusion calculations.

Re	$N = 5.96$		$N = 7.99$	
	Gaps	Bridges	Gaps	Bridges
87	554.08	513.45	195.38	177.50
348	266.32	294.35	98.37	124.76
696	205.8	223.76	75.14	105.48
870	198.14	217.17	95.42	100.35

Table 7: Source term concentration $C0$ in mol.m^{-3} for each COMSOL file

The meshing of the model was fairly simple. The part that needed the most elements was along the axis of symmetry and near the source at the inlet. Therefore, the mesh was refined along the $r = 0$ axis, with a *Maximum element size* of 0.2. For the aspect ratio of 5.96, the final mesh consisted of 46208 elements. For $N=7.99$, the same settings were used, and the total number of elements was 51520. Figure 10 pictures the meshing around the source at the bottom left corner of the geometry for $N = 5.96$. The mesh was refined to check for mesh dependency.

Satisfactory results were expected for both cases, especially for $N = 7.99$ where

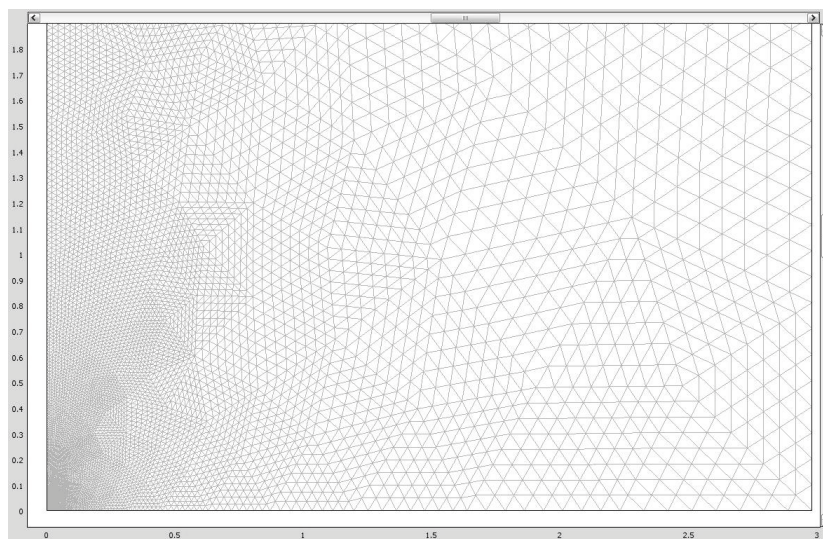


Figure 10: *Mesh of the COMSOL Convection-Diffusion, near the symmetry axis and source.*

the wall effects are not particularly of importance. In this case, classical models should be able to successfully predict the transport phenomenon.

2 Convection-Diffusion and reaction simulations

The next step in COMSOL was naturally the implementation of the isothermal reaction $CH_4 + H_2O \rightarrow CO + 3H_2$ along with a convection-diffusion model. The data used for the reaction rate implementation can be found in Appendix A. Two different models were considered, using Equations 20 and 22 for the single pellet model, 12 and 17 for the classical pseudo-heterogeneous model with effectiveness factor, all with their respective boundary conditions. The Single pellet model required a particular implementation in COMSOL, that will be described in this section.

For both models, it was decided to only use the best correlation for the Peclet number, based on the results from the dispersion calculations. Reaction was assumed to be the major factor that would effect the distribution of species anyway, which comforted us in only using one of the correlations.

2.1 Pseudo-Heterogeneous model with effectiveness factor.

The implementation of this model is simple. The geometry used consists of the same as for the dispersion calculations, without the source term at the inlet. The length of the bed is also reset accordingly to the Fluent file, without the 1.5" or 2" cut that was required when the source term was present.

The equations are specified and the reaction rate (see Appendix A) is entered as a function of the different concentrations. The reaction rate expression is based on the partial pressures of all the species. However, it was chosen to rewrite it using mass fractions. This also allows us to reduce the number of equations needed in the solid and the fluid, as the sum of mass fractions equals 1.

Both fluid and solid are modeled using a convection-diffusion model at steady state. The equations entered in the *Subdomain settings* are as follow:
Solid phase, for species $i = 1, 2, 3$:

$$D = u = v = 0$$

$$R = St_i \times (cs_i - cf_i) - \nu_i \times Da_i \times (1 - \epsilon) \times \eta_i \times \mathcal{R}(cs_i, T)$$

Fluid phase, for species $i = 1, 2, 3$:

$$D = 1/Per_i \quad 0 \quad 0 \quad 1/Pea_i$$

$$R = -St_i \times (cf_i - cs_i)$$

$$u = 0$$

$$v = 1$$

For species 4, we simply have $cs_4 = 1 - \sum_{i=1}^3 cs_i$, and $cf_4 = 1 - \sum_{i=1}^3 cf_i$. One can note that cf_i and cs_i are only really notations, and represent mass fractions. The Damkhöler number is here really defined as $Da_i = \frac{\rho d_p \bar{R}(C_{i,in}, T_{in}) M_i}{u \rho_f}$ since we base our calculations on mass fractions.

The mesh consists of 3536 triangular elements, and is refined near the wall, with a maximum element size of 0.5. The solution was checked by refining the mesh, and did not show any signs of mesh dependency. The mass balance is automatically respected, because of the set up of the problem. The mass fraction of water being

calculated as the complement to 1 of the other mass fractions. Therefore, outlet fluxes of CH_4 , H_2 and CO are compared. They can be found in Table 8.

species	3536 elts.	14144 elts.	Error (%)
CH_4	176.68	176.68	0.00
H_2	156.12	156.13	0.01
CO	78.67	78.66	0.01

Table 8: Comparison between outlet fluxes (in $g.m^{-2}.s^{-1}$ for two meshes, Pseudo-heterogeneous model.

2.2 Single Pellet model

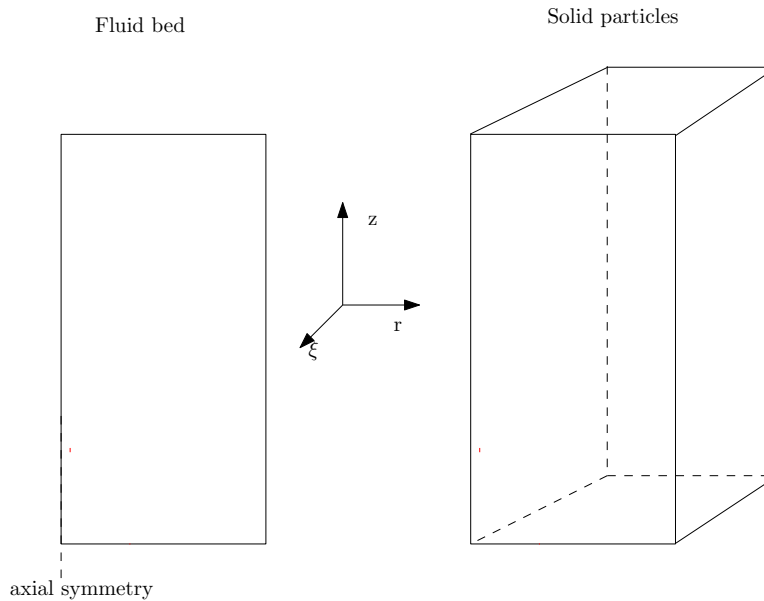


Figure 11: Geometry of the Single Pellet model.

The single pellet model requires the use of 2 geometries with coupling variables. An illustration of these geometries can be found in Figure 11. The fluid bed is modeled exactly like the bed used in the classical pseudo-heterogeneous model. For the solid, a three dimensional geometry is used, based on the fluid bed. A simple way of seeing it would be imagining that at every point of the fluid bed, a catalyst

particle is present, accordingly to the pseudo-continuum hypothesis, and that this particle is approximated by a one dimensional model.

The transport in the fluid is modeled with a convection-diffusion model at steady state, and the diffusion in the solid as a diffusion model at steady state. The implementation of the equations is done as follow:

Solid phase, for species $i = 1, 2, 3$:

$$D = 0 \quad 1$$

$$R = 2/z \times cs_i z - \Phi_i^2 \times rate$$

Fluid phase, for species $i = 1, 2, 3$:

$$D = 1/Per_i \quad 0 \quad 0 \quad 1/Pea_i$$

$$R = -St_i \times (cf_i - css_i) \times (1 - \epsilon)$$

$$u = 0$$

$$v = 1$$

For species 4, we simply have $cs_4 = 1 - \sum_{i=1}^3 cs_i$, $css_4 = 1 - \sum_{i=1}^3 css_i$, and $cf_4 =$

$1 - \sum_{i=1}^3 cf_i$. css_i represents the solid surface molecular weight of species i , and is obtained through extrusion coupling variable from the boundary $z=1$ of the 3D solid geometry to be applied to the entire 2D fluid geometry.

The mesh of the 2D geometry is similar to the one used in the simple pseudo-heterogenous model. It was simplified, with only 2240 elements, and no particular refinements near the walls. For the 3D mesh, a boundary layer of 20 layers was placed next to the particles surface, with a total number of elements of 2383.

Part IV

Results and discussion

1 Dispersion model

The validity of the classical Reaction Engineering models were tested by comparing the concentration distribution between COMSOL and Fluent for two different positions in the bed.

For $N = 5.96$, concentration profiles were extracted from Fluent at $z=5''$ and $10''$ from the inlet, so at $z=3.5''$ and $8.5''$ from the source. Therefore the COMSOL profiles were obtained at $z=3.5''$ and $8.5''$. This was repeated for each Reynolds number and for both configurations of the Fluent file.

For $N = 7.99$, the concentration profiles were extracted at $z=12''$ and $7''$ from the inlet, so at $z=10''$ and $5''$ from the source. Accordingly, the COMSOL profiles were obtained at $z=10''$ and $5''$.

In order to get the concentration profiles in Fluent at these two positions, iso-clips were created. First, full radial surfaces were created on the total length of the bed, at $Xi = 0.0005, 0.0015, 0.0025, 0.004$, and 0.01 to 2.88 for $N = 5.96$ or 0.01 to 3.89 for $N = 7.99$ with an interval of 0.01 . These cylinders were then clipped to the corresponding position of the bed by creating new iso-clip surfaces of $2mm$ thickness. The creation of iso-clips failed near the center of the bed several times, due to the presence of a particle at the center of the bed. Figure 12 shows the two surfaces for the tube of $N = 7.99$, with gaps configuration. Then a *Surface integral Mass-average* computation of the concentration of CH_4 was done on these surfaces, to obtain an average of the concentration along the bed radius at the defined positions.

The concentration profiles from COMSOL were simply extracted with a cross-sectional area plot. All the data were treated on Excel.

The convection-diffusion model was tested with different correlations for the axial and radial Peclet numbers. These correlations are given by Equations 4 - 9. The values obtained by Magnico were also tested. All the values that were computed for the Peclet numbers $Pe_{m,r}$ and $Pe_{m,a}$ can be found in Appendix B. None of them rely on the particle or bed diameter, and therefore they are the same for the two beds.

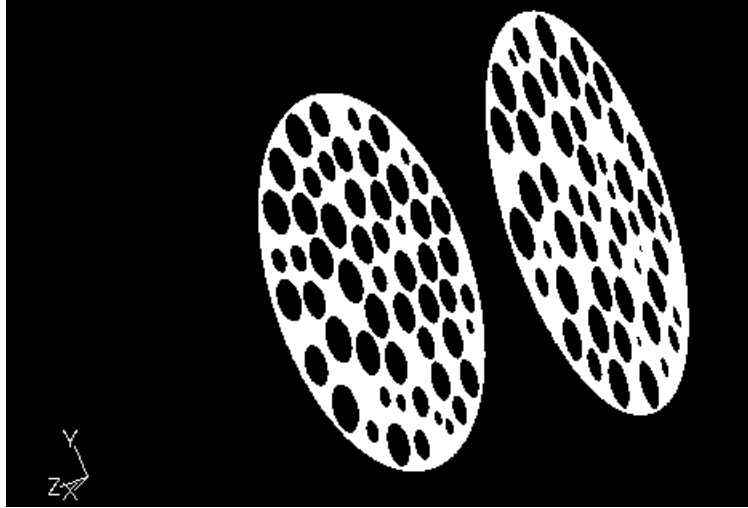


Figure 12: *Iso-clips created on Fluent at $z=7''$ and $12''$ for $N = 7.99$.*

1.1 Packed bed of $N = 5.96$

First of all, we need to verify the validity of the COMSOL files, and this is done by checking that the fluxes of CH_4 at the outlet are the same for Fluent and COMSOL for every Reynolds. This serves as a test to verify that the concentrations we calculated for the source are correct. Table 9 regroups all the values. They were obtained in Fluent by simply dividing the CH_4 mass flowrate at the outlet by the outlet surface. The COMSOL values were obtained with a boundary integration.

Re	Configuration	Fluent	COMSOL	Error (%)
87	Gaps	0.0310	0.0313	0.96
	Bridges	0.0287	0.0290	1.03
348	Gaps	0.0596	0.0602	1.00
	Bridges	0.0659	0.0666	1.05
696	Gaps	0.0921	0.0931	1.09
	Bridges	0.100	0.101	0.99
870	Gaps	0.111	0.112	0.89
	Bridges	0.122	0.123	0.81

Table 9: *Outlet fluxes (in $g.m^{-2}.s^{-1}$) of CH_4 for Fluent and COMSOL for $N=5.96$*

Figures 13 - 28 show all the concentration profiles for the $N = 5.96$ bed. The dashed line represents the profile obtained with CFD on Fluent, and the plain lines

represent the profiles obtained with the diffusion model on COMSOL with the various correlations for the Peclet numbers. In blue is the one by Coelho et al., green is the one by Freund et al., red by Foumeny et al., and orange by Magnico.

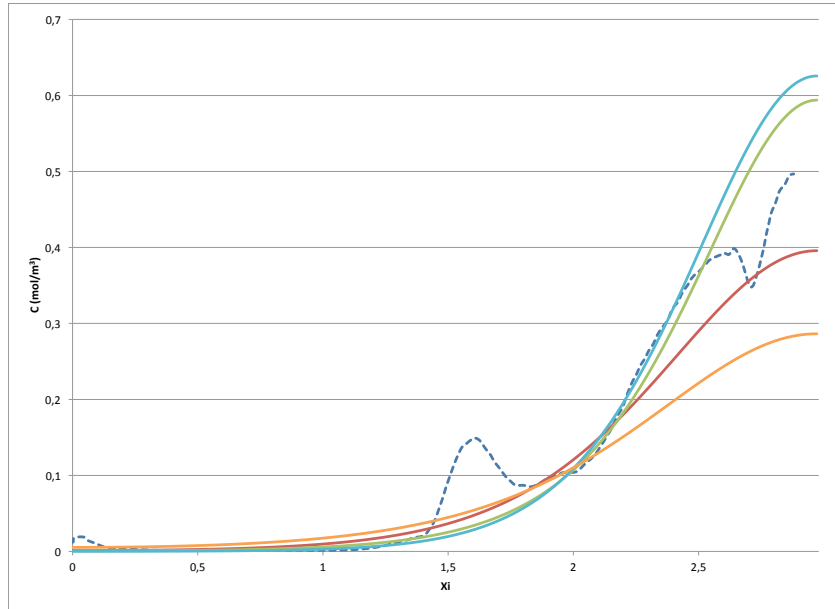


Figure 13: *Concentration profile of CH_4 at $z=5''$ for $N = 5.96$, $Re=87$, Gaps configuration.*

The first comment that can be done when looking at these results, is that clearly some of the correlations we discussed in Part I do not fit our case of low aspect ratio bed. The values of Pe_r and Pe_a obtained with Equations 8 and 9 from Coelho et al. [4], as well as with Equations 6 and 7 from Freund et al. [10] lead to an incorrect simulation of dispersion. Indeed, for every Reynolds - with the exception of $Re=87$ - and for both gaps and bridges configurations, these correlations lead to values of the Peclet numbers that underestimate greatly radial dispersion. Axial dispersion is also under-evaluated, even though not as much as the radial one. The values for the Peclet numbers can be found in Appendix A. The correlations developed by Freund et al. were suited for smaller Peclet numbers, which could certainly explain the invalidity of the results.

At low Reynolds it seems that the correlations obtained by Coelho et al. and Freund et al. fit the CFD results better. When increasing the Reynolds number however, the correlations for Peclet number by Foumeny et al. and the values proposed by Magnico seem to be more accurate, even though they show too much axial

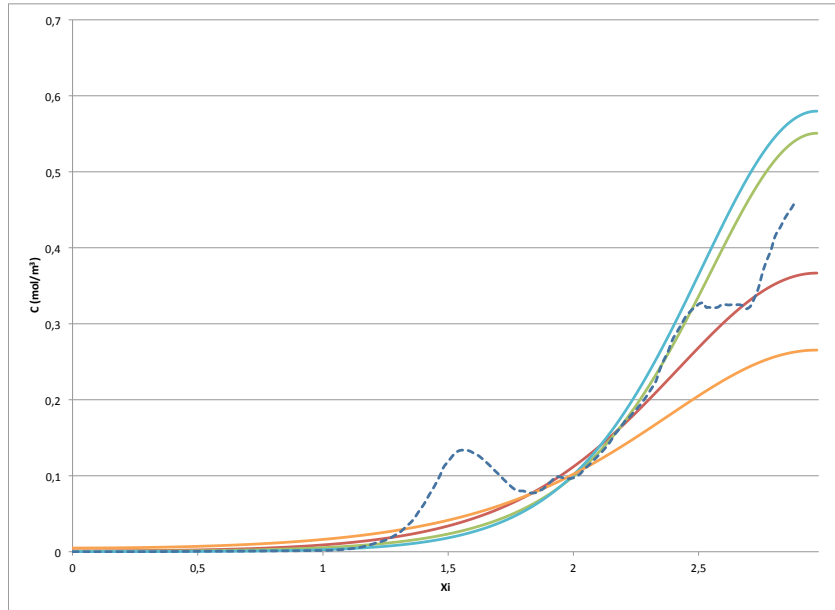


Figure 14: Concentration profile of CH_4 at $z=5''$ for $N = 5.96$, $Re=87$, Bridges configuration.

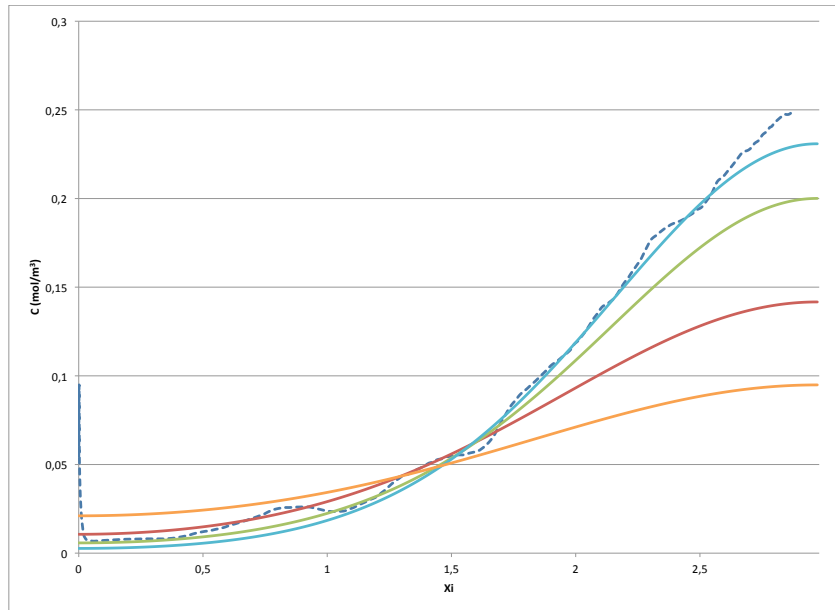


Figure 15: Concentration profile of CH_4 at $z=10''$ for $N = 5.96$, $Re=87$, Gaps configuration.

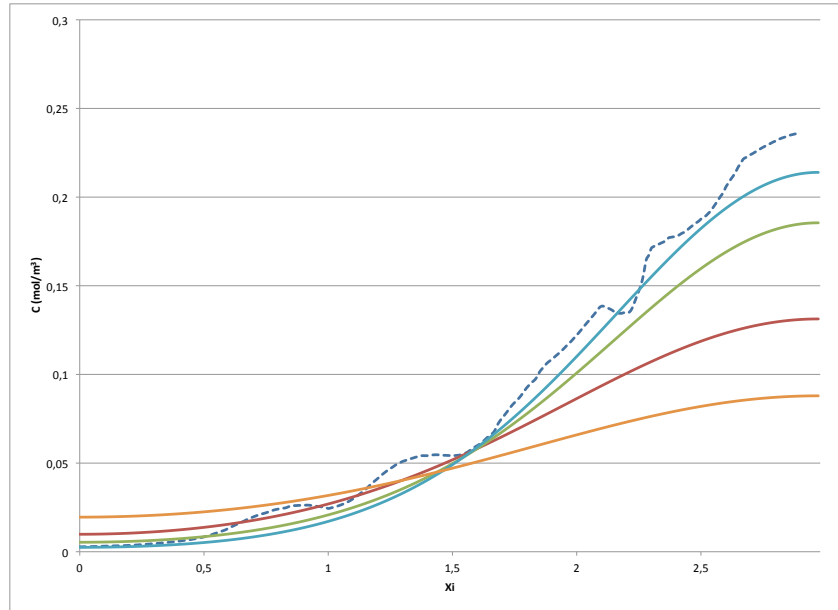


Figure 16: Concentration profile of CH_4 at $z=10''$ for $N = 5.96$, $Re=87$, Bridges configuration.

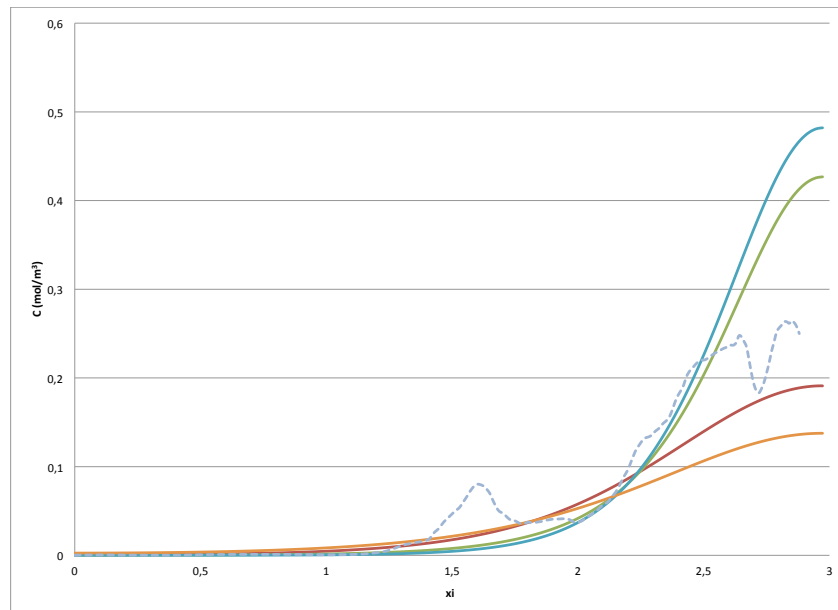


Figure 17: Concentration profile of CH_4 at $z=5''$ for $N = 5.96$, $Re=348$, Gaps configuration.

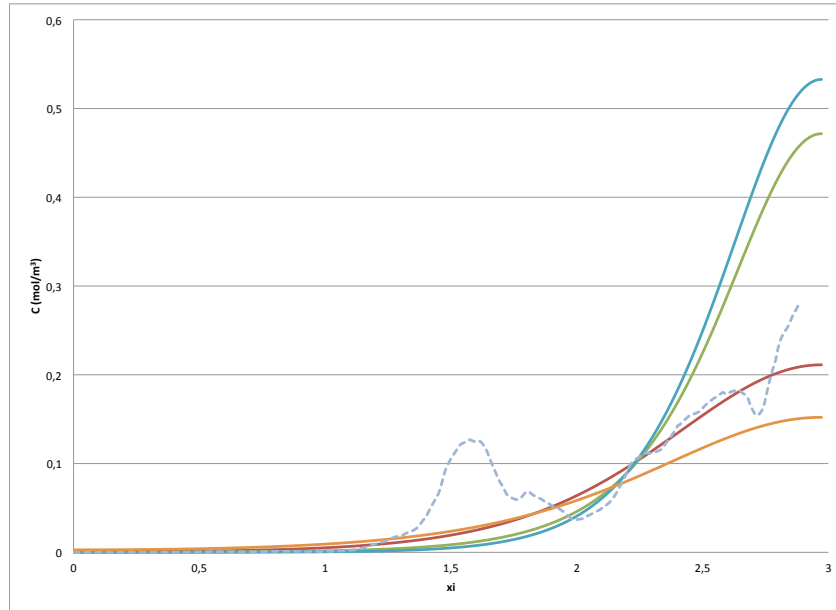


Figure 18: Concentration profile of CH_4 at $z=5''$ for $N = 5.96$, $Re=348$, Bridges configuration.

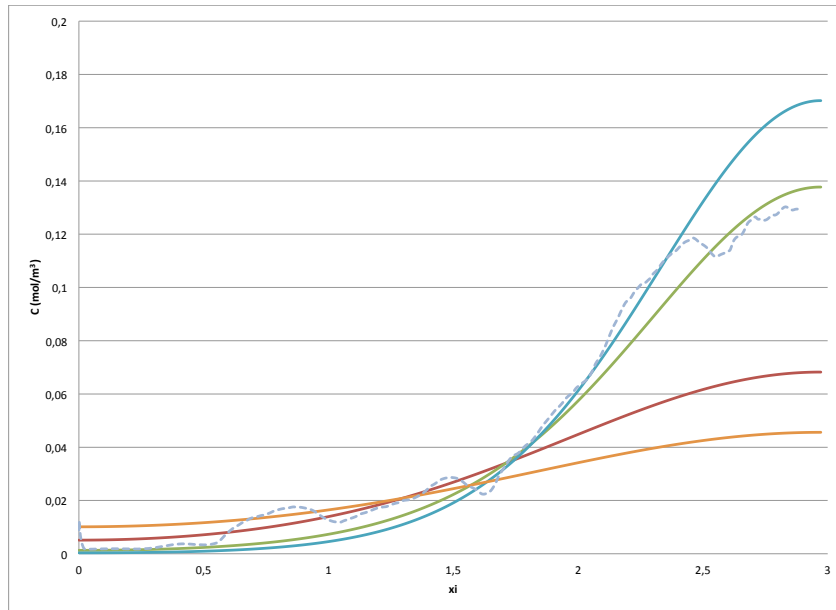


Figure 19: Concentration profile of CH_4 at $z=10''$ for $N = 5.96$, $Re=348$, Gaps configuration.

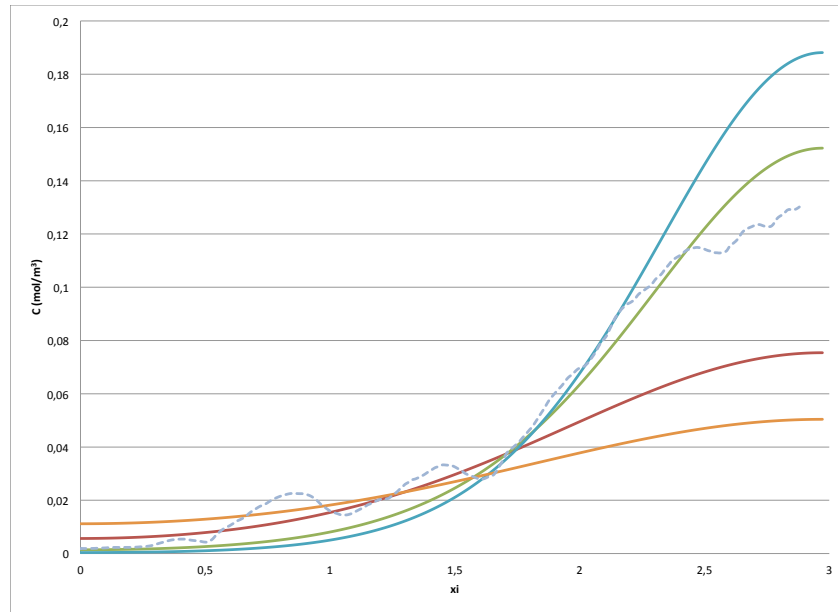


Figure 20: Concentration profile of CH_4 at $z=10''$ for $N = 5.96$, $Re=348$, Bridges configuration.

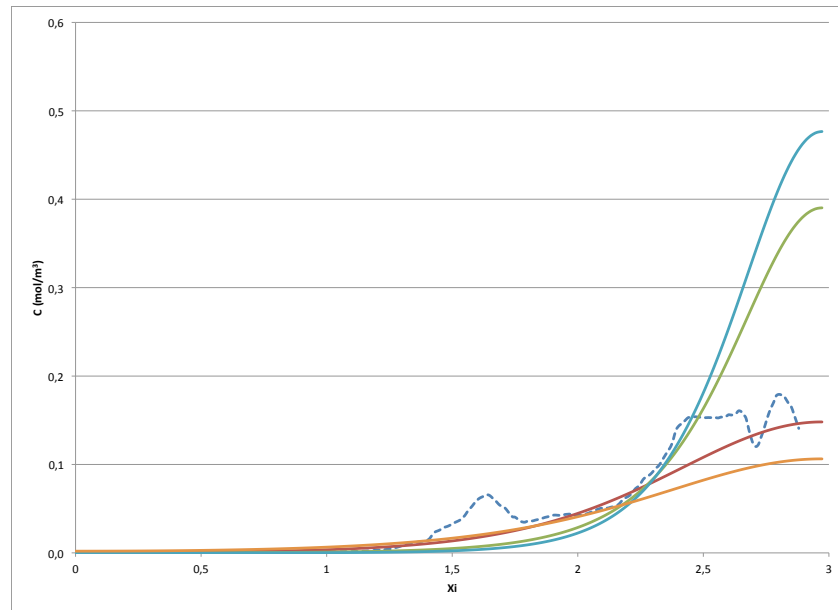


Figure 21: Concentration profile of CH_4 at $z=5''$ for $N = 5.96$, $Re=696$, Gaps configuration.

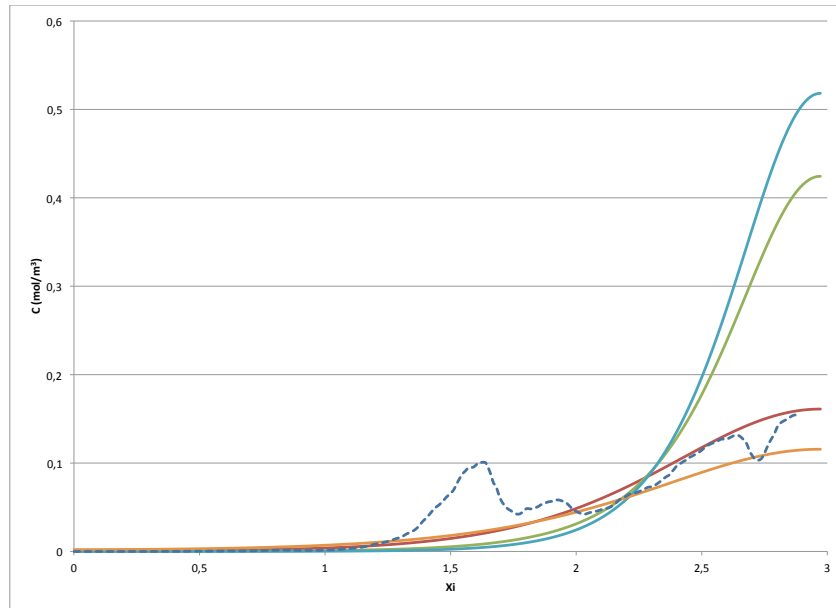


Figure 22: Concentration profile of CH₄ at z=5'' for N = 5.96, Re=696, Bridge configuration.

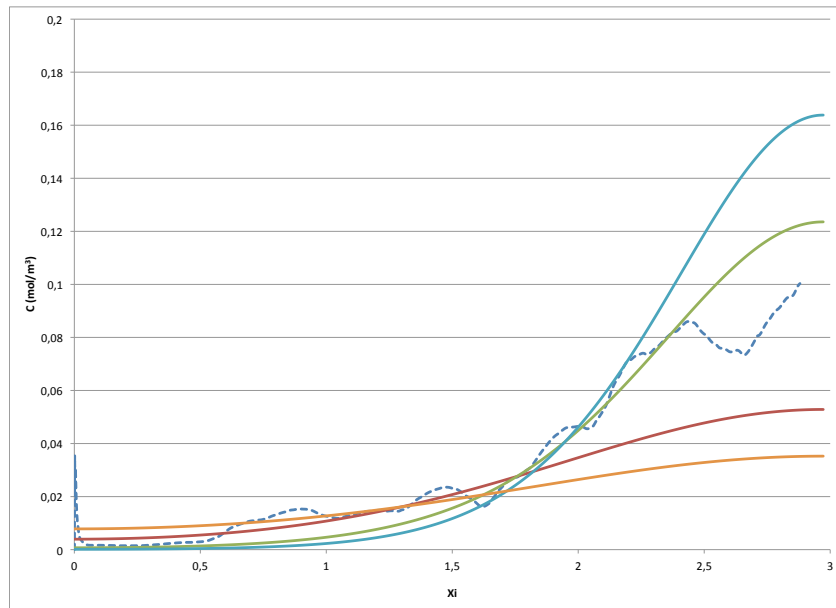


Figure 23: Concentration profile of CH₄ at z=10'' for N = 5.96, Re=696, Gaps configuration.

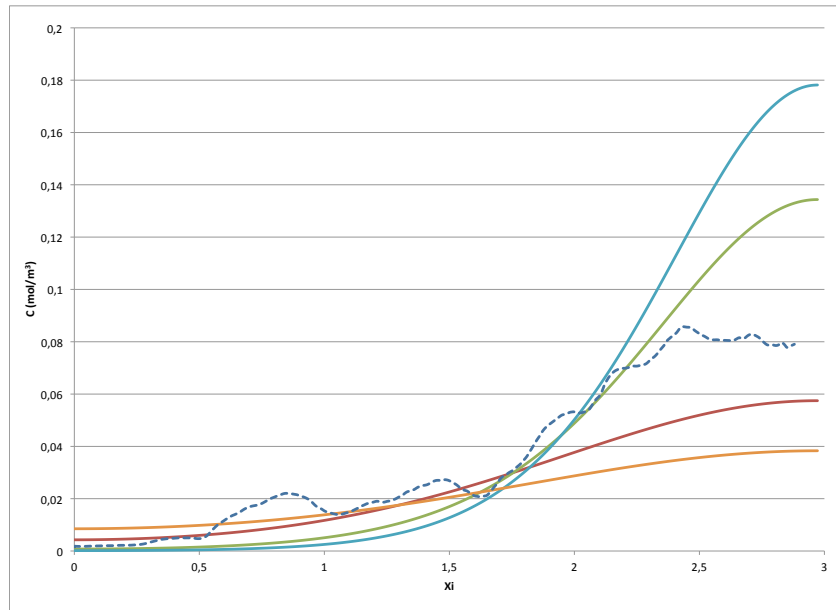


Figure 24: Concentration profile of CH_4 at $z=10''$ for $N = 5.96$, $Re=696$, Bridges configuration.

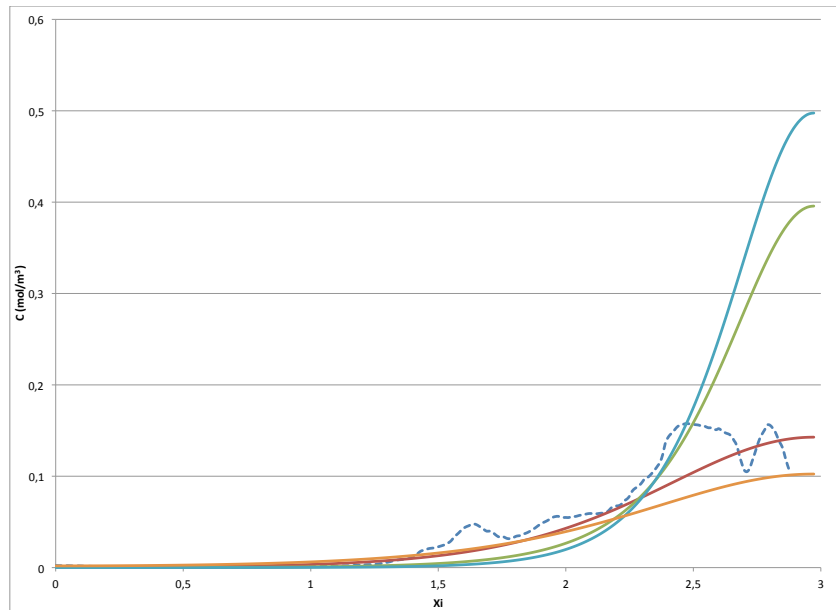


Figure 25: Concentration profile of CH_4 at $z=5''$ for $N = 5.96$, $Re=870$, Gaps configuration.

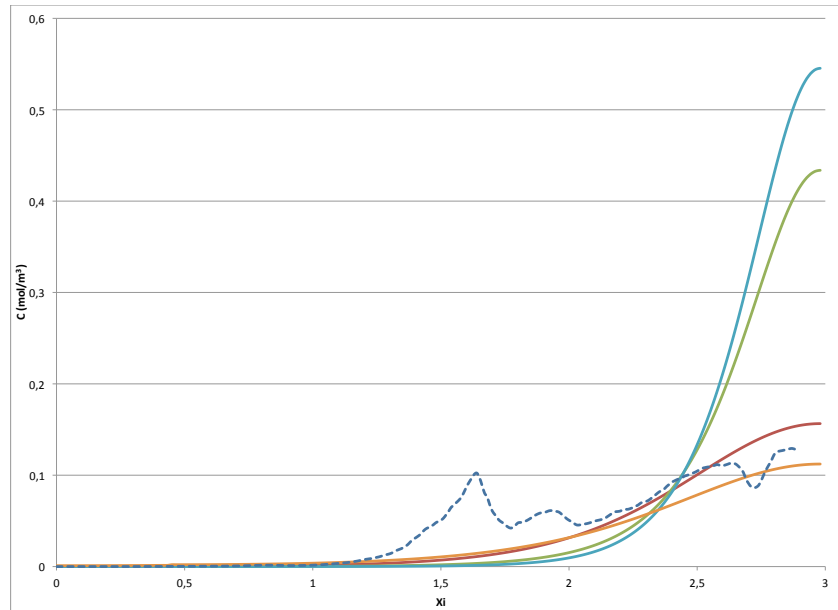


Figure 26: Concentration profile of CH_4 at $z=5''$ for $N = 5.96$, $Re=870$, Bridges configuration.

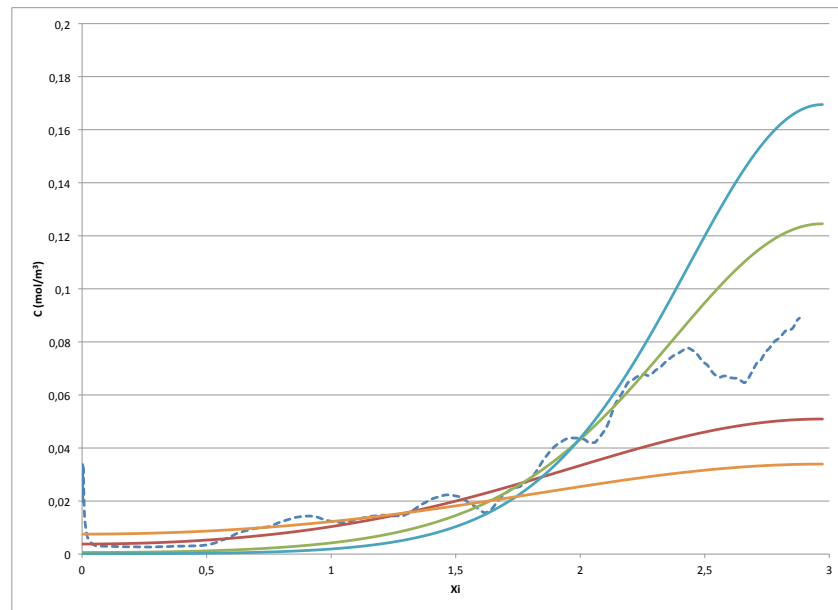


Figure 27: Concentration profile of CH_4 at $z=10''$ for $N = 5.96$, $Re=870$, Gaps configuration.

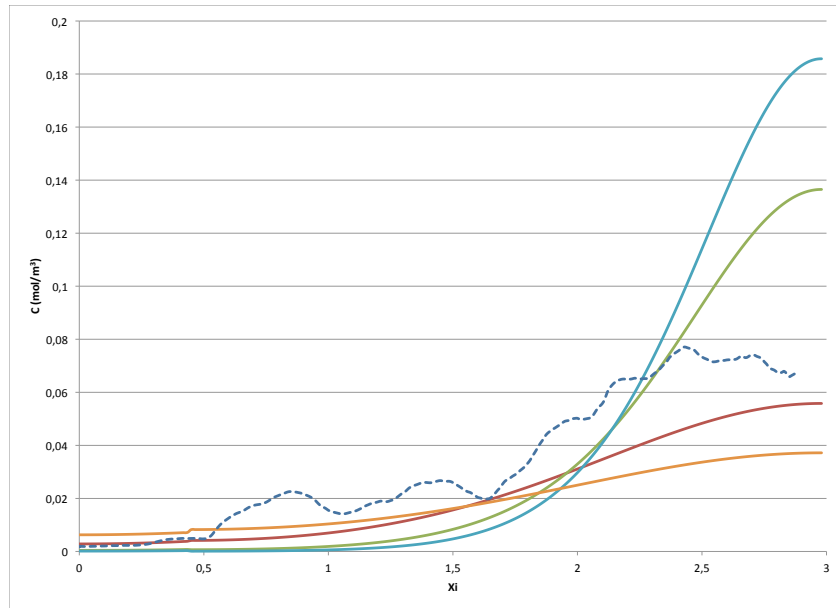


Figure 28: Concentration profile of CH_4 at $z=10''$ for $N = 5.96$, $Re=870$, Bridges onfiguration.

dispersion. Magnico's results were suited for Reynolds between 7 and 200, but still show good results at higher Reynolds numbers.

One can realize when looking at the graphs that there are differences between the Fluent profiles for gaps and bridges configurations. Indeed, for $N = 5.96$ the gap configuration showed a tendency to develop build-ups of CH_4 in the gaps between the wall and the particles, as can be spotted on Figure 23 and 27 near $\xi=0$. None of the profiles we obtained with the bridges configuration showed this behavior. This phenomenon was moreover spotted when looking at concentration distribution on the mid-plane of the tube for the gaps configuration (one of those artifact was pictured previously on Figure 6). However, when comparing fluxes of CH_4 at different positions in the bed, no significant difference was spotted in any of the files, which confirms the insignificant impact of these artifacts on our study.

At this value of N , there is enough dispersion for CH_4 to start reaching the walls, which puts us in a position where wall effects on velocity have to be considered. These effects might explain the global lack or excess (depending on the correlation) of axial dispersion of the models, but in order to fully understand and verify the phenomenon, a longer bed would be required. And in that case, computational power limits us in our research.

The overall shapes of the profiles obtained with reaction engineering models match the one obtained with CFD calculations. In order to get a finer comparison, more runs of CFD calculations, with different beds of same aspect ratio would be needed, to get an average of the concentration profile with Fluent. Also, several points of injection could be considered, near the wall, or at mid distance between the wall and the symmetry axis. This last modification could also be a way to evaluate the assumption of symmetry in this kind of bed.

1.2 Packed bed of $N = 7.99$

Just like for $N = 5.96$, we first verified that the source terms implemented in COMSOL were in agreement with the Fluent files. This was done again by looking at the outlet fluxes in each file. The results are given in Table 10.

Re	Configuration	Fluent	COMSOL	Error (%)
87	Gaps	0.00606	0.00612	0.98
	Bridges	0.00552	0.00556	0.72
348	Gaps	0.0122	0.0123	0.81
	Bridges	0.0155	0.0156	0.64
696	Gaps	0.0187	0.0188	0.53
	Bridges	0.0263	0.0264	0.38
870	Gaps	0.0296	0.0299	1.00
	Bridges	0.0312	0.0314	0.64

Table 10: *Outlet fluxes (in $g.m^{-2}.s^{-1}$) of CH_4 for Fluent and COMSOL for $N=7.99$*

Figures 29 - 44 show all the concentration profiles for the $N = 7.99$ bed. The dashed line represents the profile obtained with CFD on Fluent, and the plain lines represent the profiles obtained with the diffusion model on COMSOL with the various correlations for the Peclet numbers. In blue is the one by Coelho et al., green is the one by Freund et al., red by Foumeny et al., and orange by Magnico.

It clearly appears that the prediction by Magnico do not stand in this case, as the values he proposed for the case of $N = 7.3$ appear to lead to an overestimation of both radial and axial dispersion, with the concentration profile being both too flat and too high at the wall. Indeed, he predicted values of $Pe_r = 5$ and $Pe_a = 1$, and when looking at Appendix A, it appears clearly that these values, particularly Pe_r are in total disagreement with the rest of the literature. On another hand, none of these values take into account the bed-to-particle diameter ratio like his do.

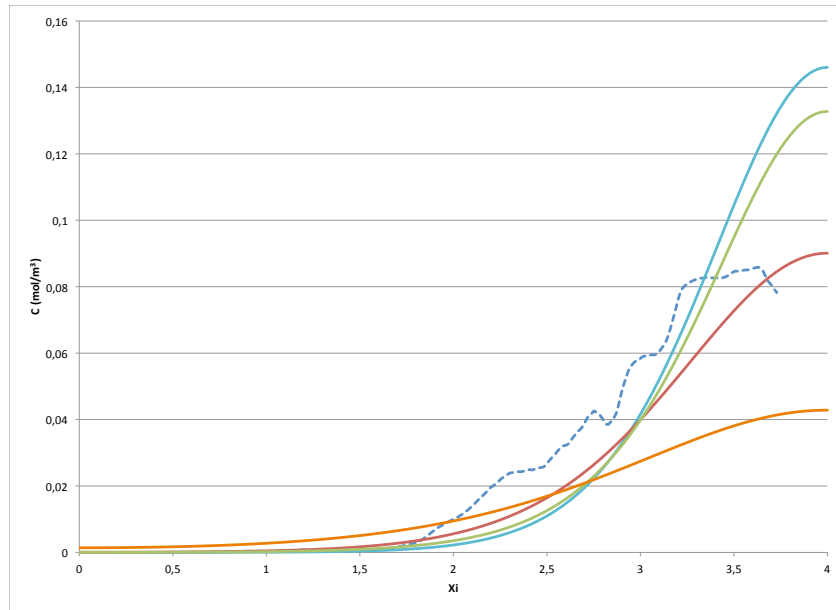


Figure 29: Concentration profile of CH_4 at $z=7''$ for $N = 7.99$, $Re=87$, Gaps configuration.

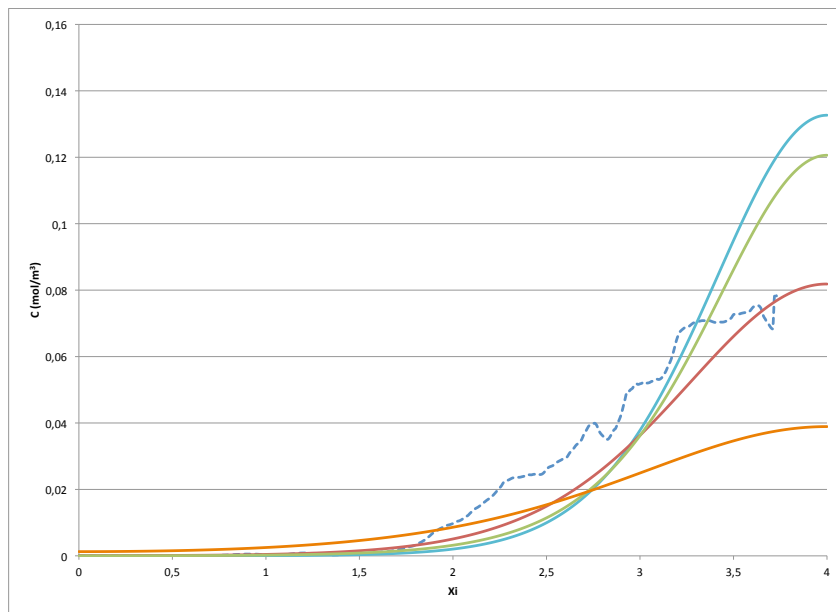


Figure 30: Concentration profile of CH_4 at $z=7''$ for $N = 7.99$, $Re=87$, Bridges configuration.

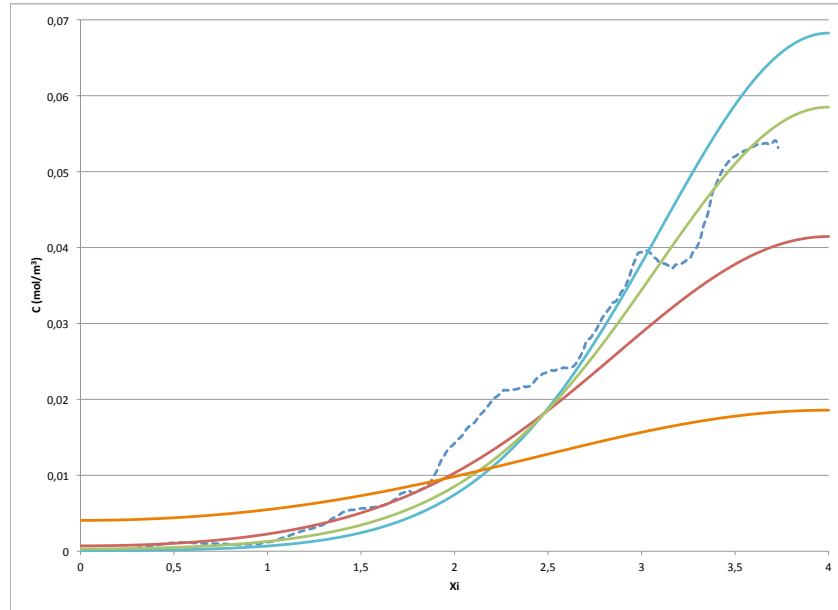


Figure 31: Concentration profile of CH_4 at $z=12''$ for $N = 7.99$, $Re=87$, Gaps configuration.

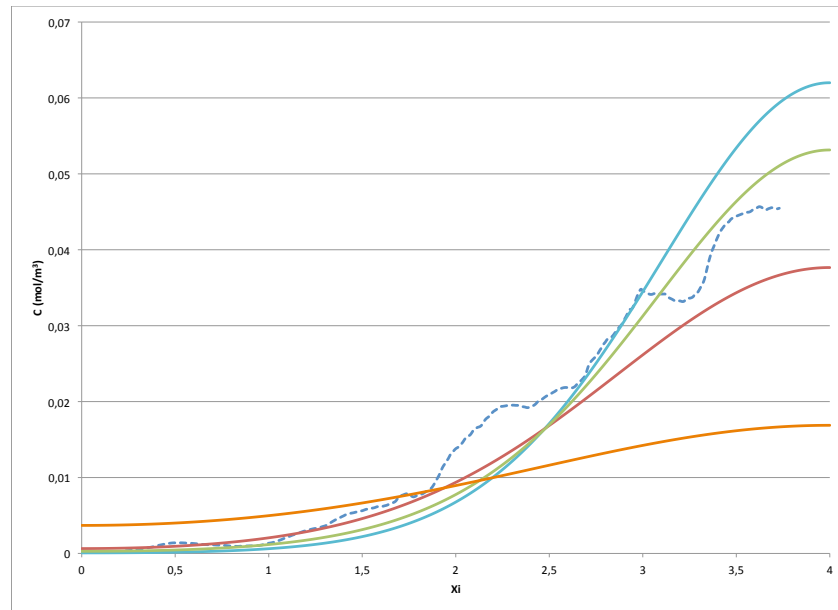


Figure 32: Concentration profile of CH_4 at $z=12''$ for $N = 7.99$, $Re=87$, Bridges configuration.

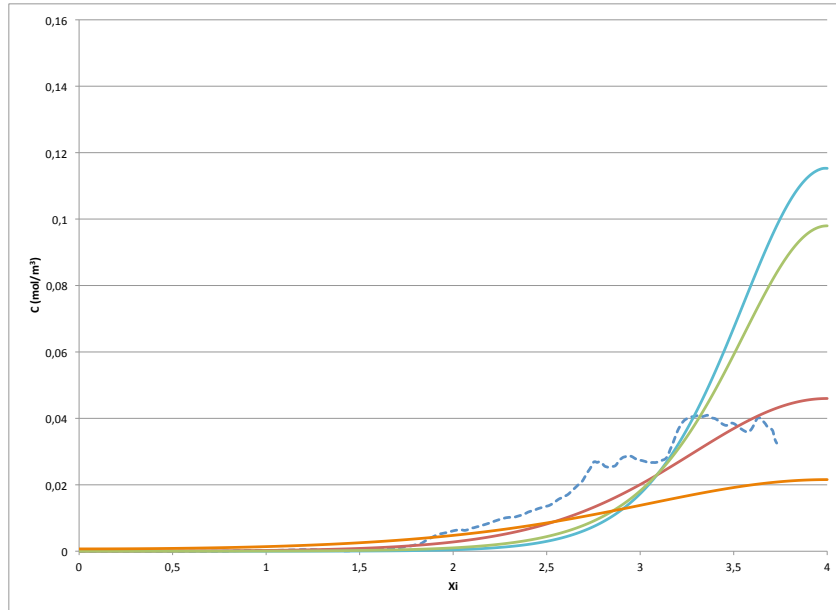


Figure 33: Concentration profile of CH_4 at $z=7''$ for $N = 7.99$, $Re=348$, Gaps configuration.

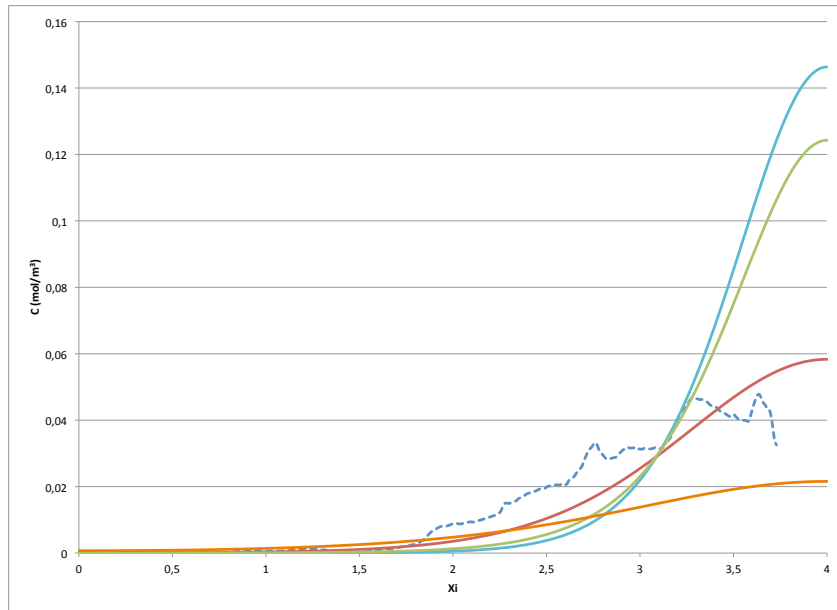


Figure 34: Concentration profile of CH_4 at $z=7''$ for $N = 7.99$, $Re=348$, Bridges configuration.

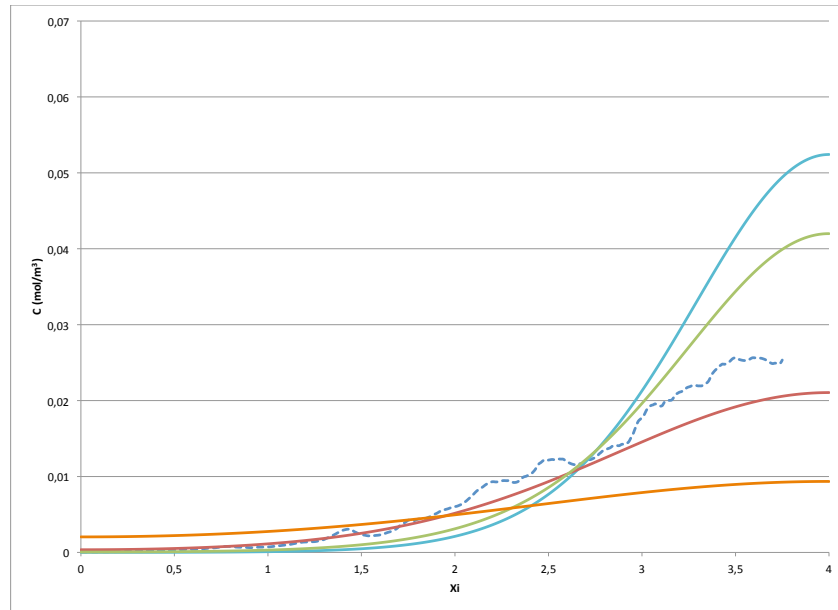


Figure 35: Concentration profile of CH_4 at $z=12''$ for $N = 7.99$, $Re=348$, Gaps configuration.

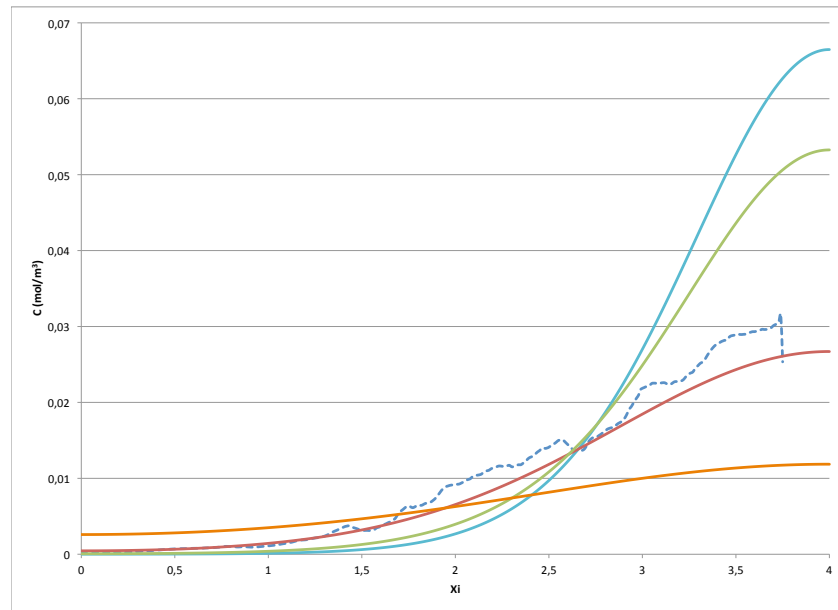


Figure 36: Concentration profile of CH_4 at $z=12''$ for $N = 7.99$, $Re=348$, Bridges configuration.

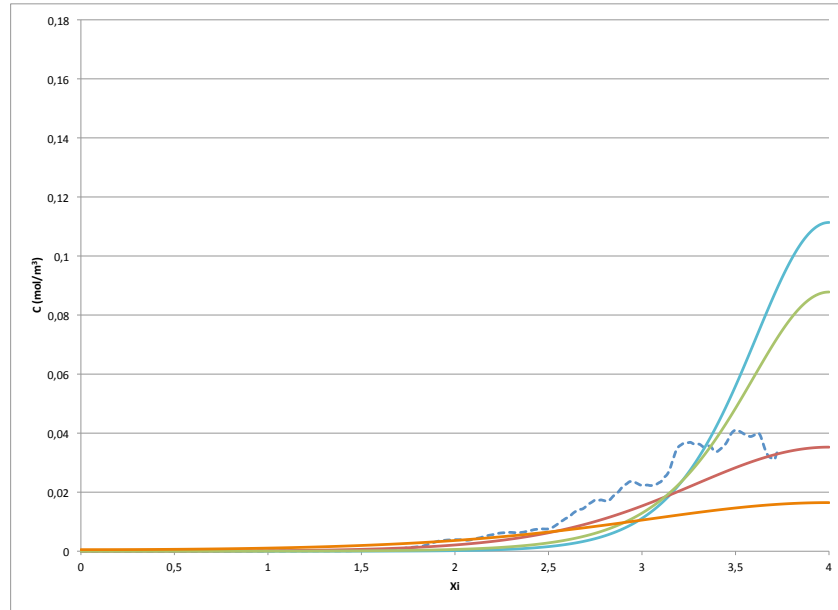


Figure 37: Concentration profile of CH_4 at $z=7''$ for $N = 7.99$, $Re=696$, Gaps configuration.

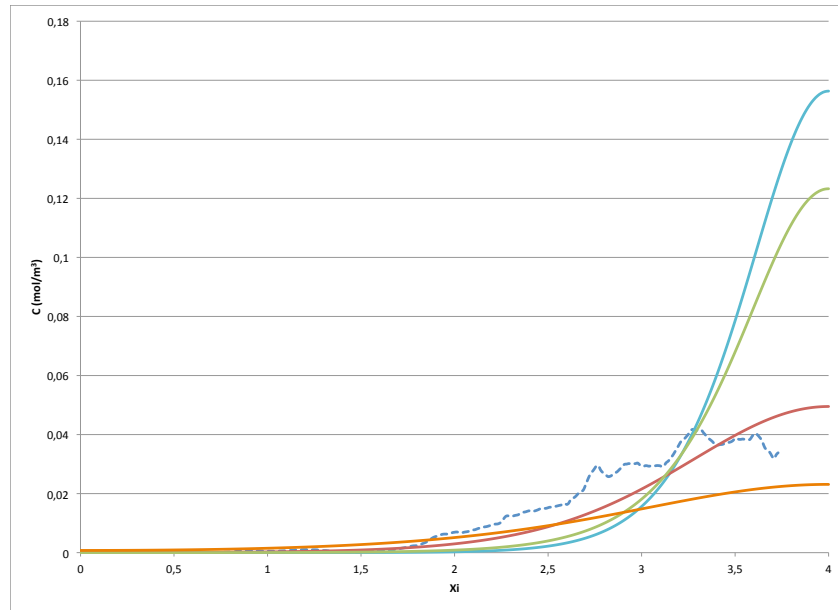


Figure 38: Concentration profile of CH_4 at $z=7''$ for $N = 7.99$, $Re=696$, Bridges configuration.

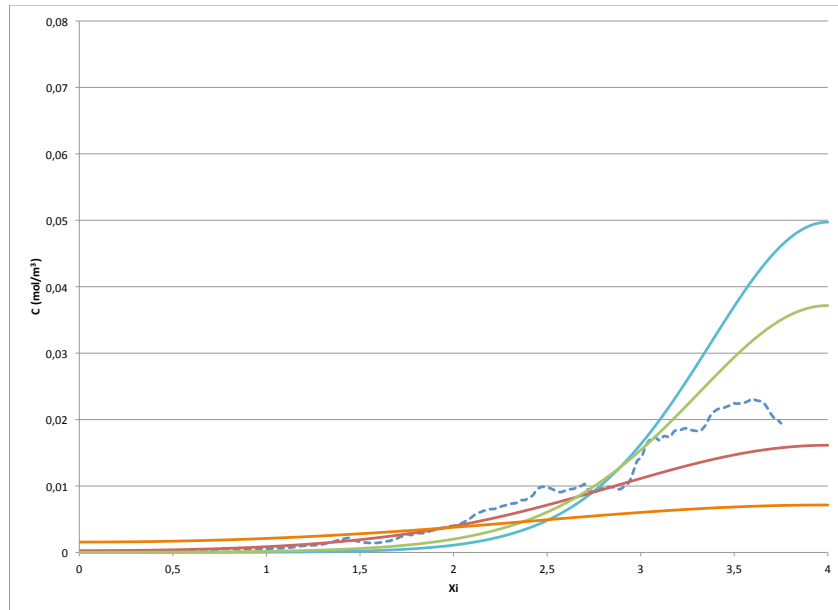


Figure 39: Concentration profile of CH_4 at $z=12''$ for $N = 7.99$, $Re=696$, Gaps configuration.

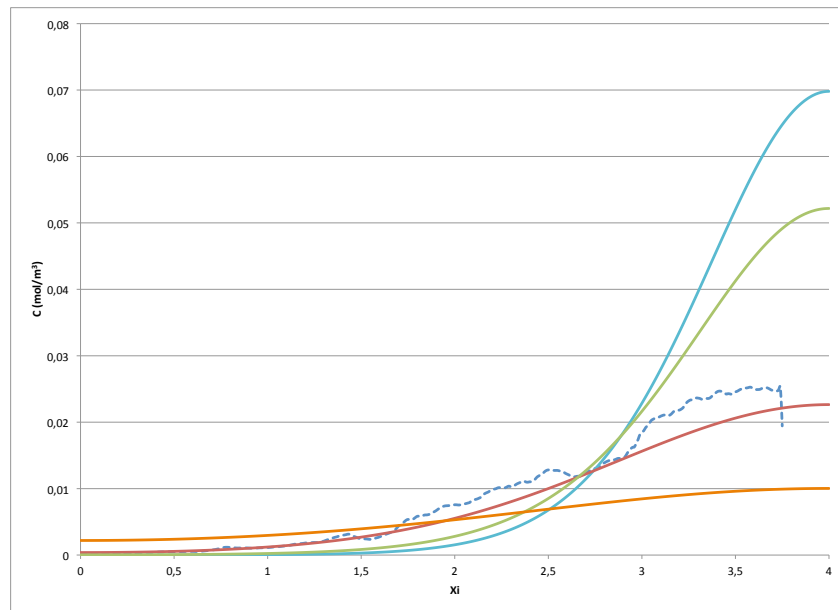


Figure 40: Concentration profile of CH_4 at $z=12''$ for $N = 7.99$, $Re=696$, Bridges configuration.

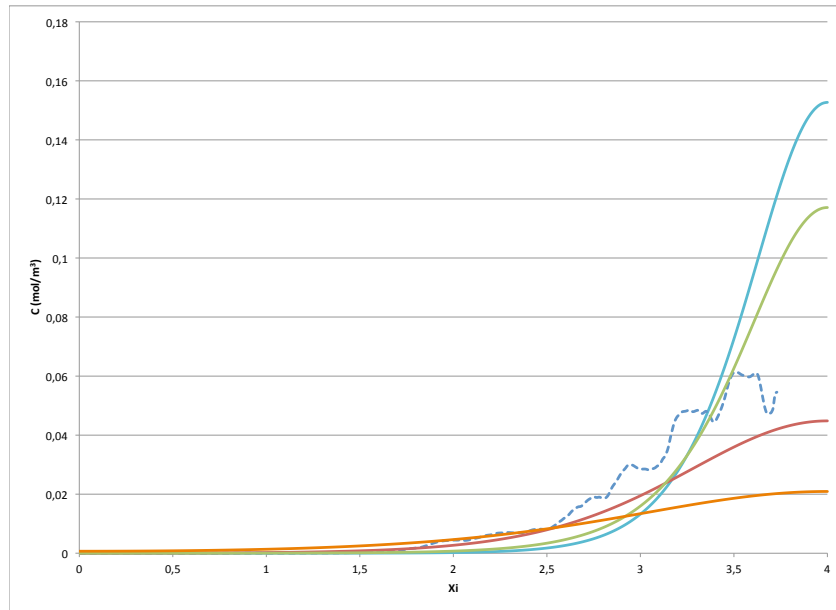


Figure 41: Concentration profile of CH_4 at $z=7''$ for $N = 7.99$, $Re=870$, Gaps configuration.

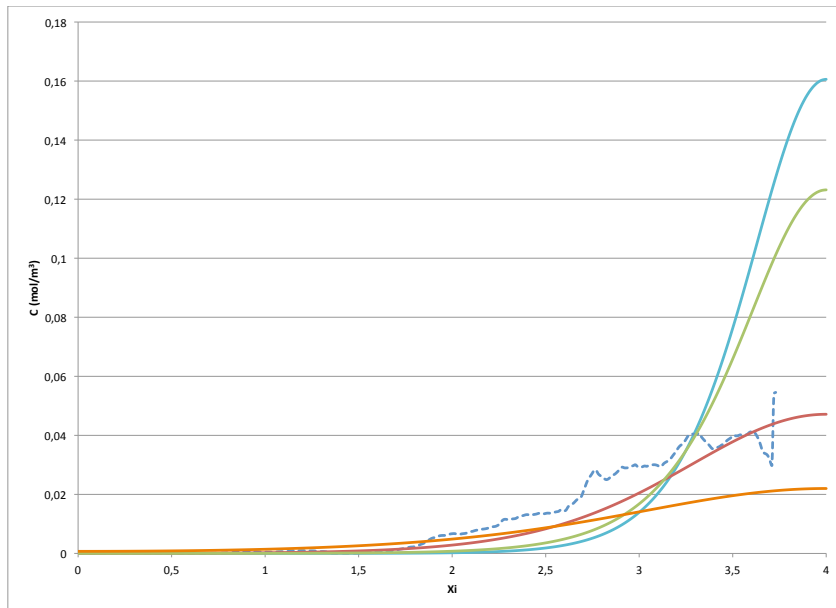


Figure 42: Concentration profile of CH_4 at $z=7''$ for $N = 7.99$, $Re=870$, Bridges configuration.

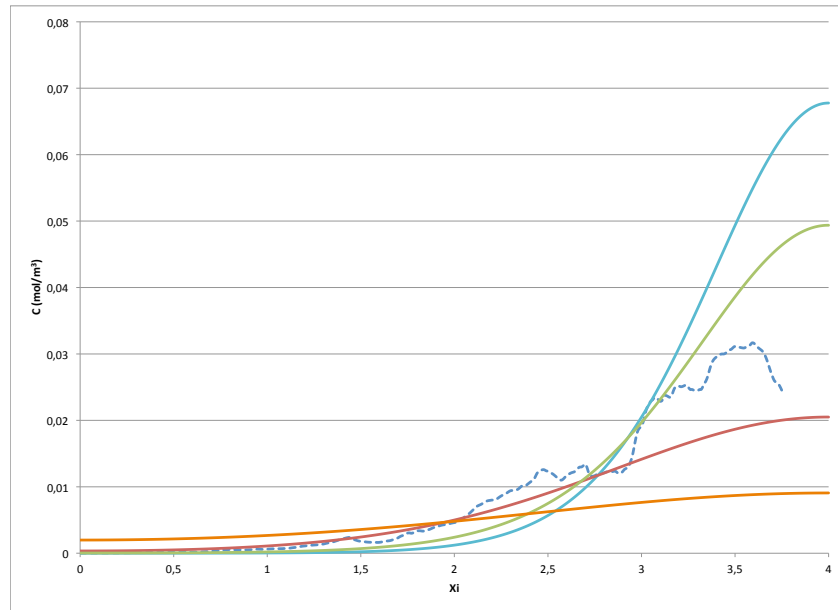


Figure 43: Concentration profile of CH_4 at $z=12''$ for $N = 7.99$, $Re=870$, Gaps configuration.

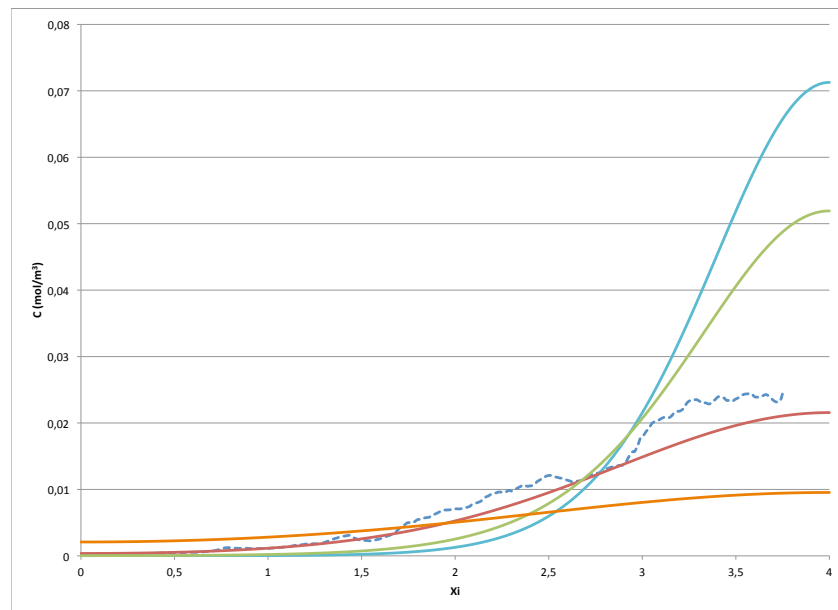


Figure 44: Concentration profile of CH_4 at $z=12''$ for $N = 7.99$, $Re=870$, Bridges configuration.

As observed in the case of $N = 5.96$, both correlations by Freund et al. and Coelho et al. underestimate the radial dispersion for $N = 7.99$. However, the correlations by Foumeny et al. seems to fit the Fluent data for all Reynolds number, and for both gaps and bridges configurations. A particularly good agreement is observed for the bridges configuration, especially at higher Reynolds numbers.

The case of $N = 7.99$ presents a high enough N to assume that the wall effect should not be of high impact on the overall transfer mechanisms in the bed, and the dispersion model should give results comparable with the CFD calculations. This is indeed the case when considering the values of Peclet numbers obtained with the Foumeny et al. correlations.

1.3 Implementation of the velocity and porosity profiles $u(r)$ and $\epsilon(r)$

The porosity profiles were extracted for both N and for both configurations of the mesh, calculating the Area occupied by the fluid in each radial surface in Fluent. They can be found in Figure 45 and 46.

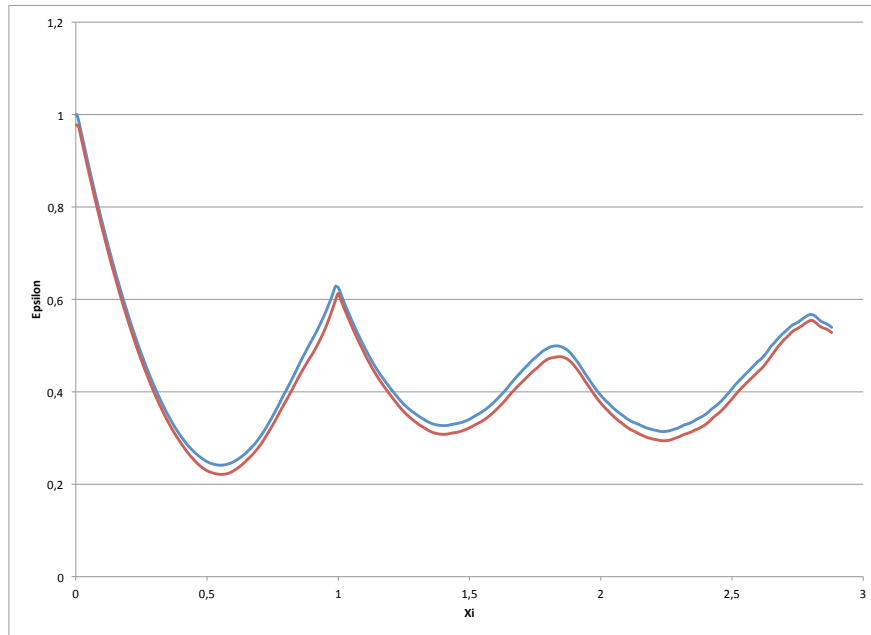


Figure 45: *Porosity profile for $N = 5.96$. Red: Bridges, Blue: Gaps*

As expected, the porosity profile obtained for the bridges configuration is lower

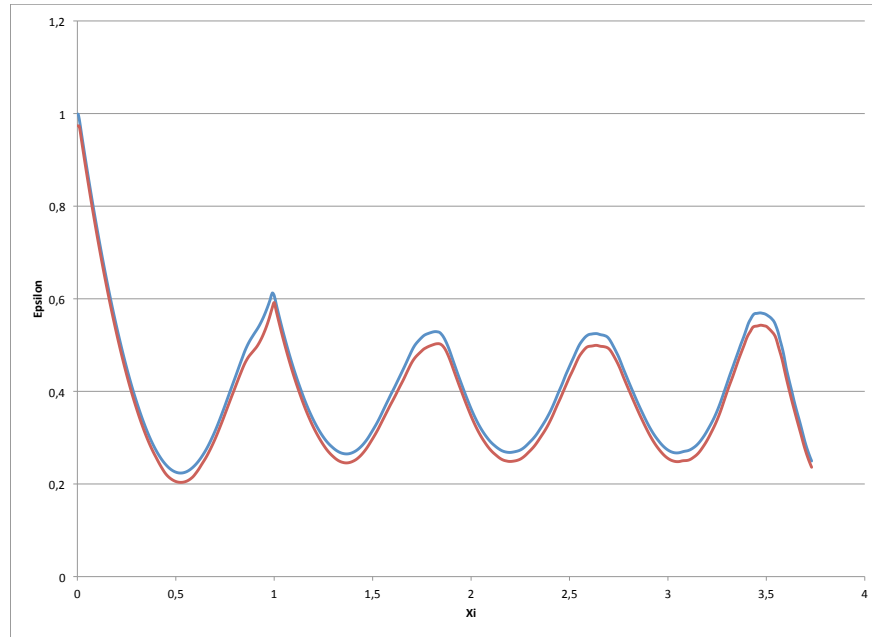


Figure 46: *Porosity profile for $N = 7.99$. Red: Bridges, Blue: Gaps*

than the one with gaps. These profiles compare well with the literature for $N = 5.96$ [21]. The mean values of the porosity are 0.44 and 0.42 for $N = 5.96$ and 0.41 and 0.39 for $N = 7.99$, for gaps and bridges configurations respectively.

Interstitial velocity profiles were extracted for every Reynolds number. Using the same surfaces as for the porosity profile, the mean velocity magnitude was computed and averaged (based on mass) on all of these radial surfaces. An example is given in Figure 47 for $Re = 348$ and $N = 5.96$.

Both the velocity and porosity profiles were implemented in COMSOL, in order to evaluate the impact of a velocity profile in the dispersion models. These models are based on superficial velocity, and when computing this velocity from the porosity and interstitial velocity profile, we could observe a relatively flat profile. The concentration profiles were slightly affected, as pictured on Figures 48 - 53. These profiles were obtained using the $N = 5.96$ tube and $Re = 348$ for both gaps and bridges configurations. The legend is as follows: Dashed red: Fluent Bridges, dashed blue: Fluent gaps, purple: Bridges, green: Gaps, orange: Bridges + profiles, blue: Gaps + profiles.

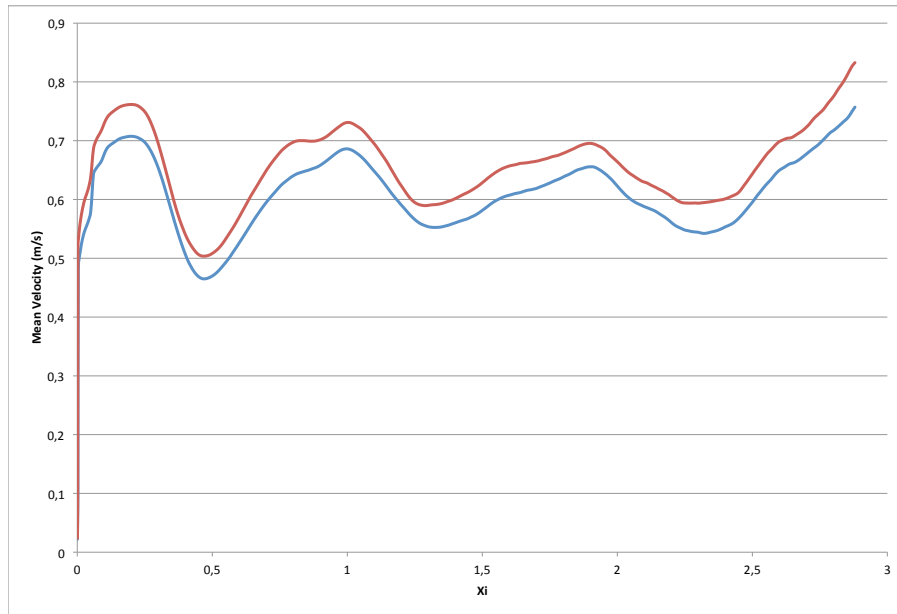


Figure 47: Mean velocity profile for $N = 5.96$, $Re = 348$, Red: Bridges, Blue: Gaps

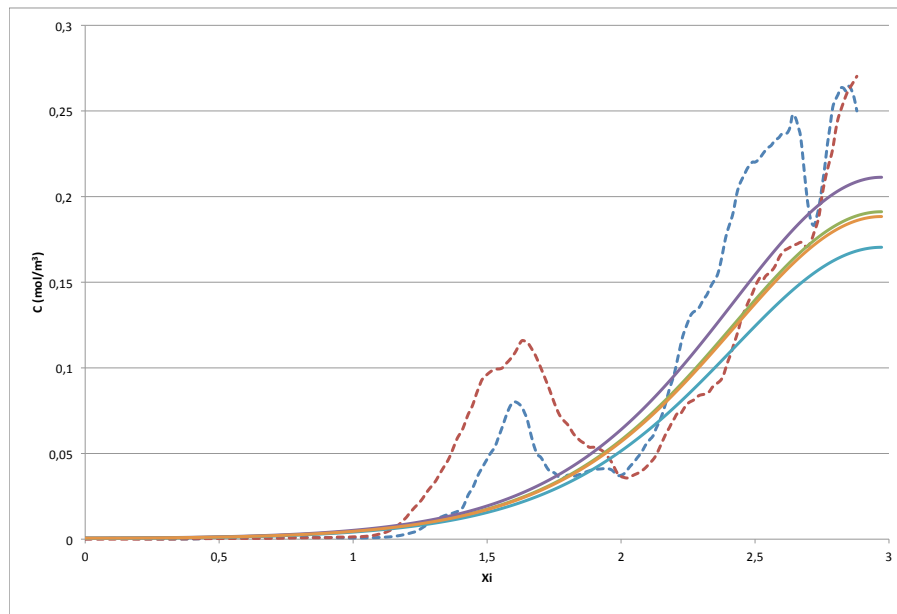


Figure 48: Concentration profiles for $N = 5.96$, $Re = 348$, correlation by Foumeny et al. at $z'=5$

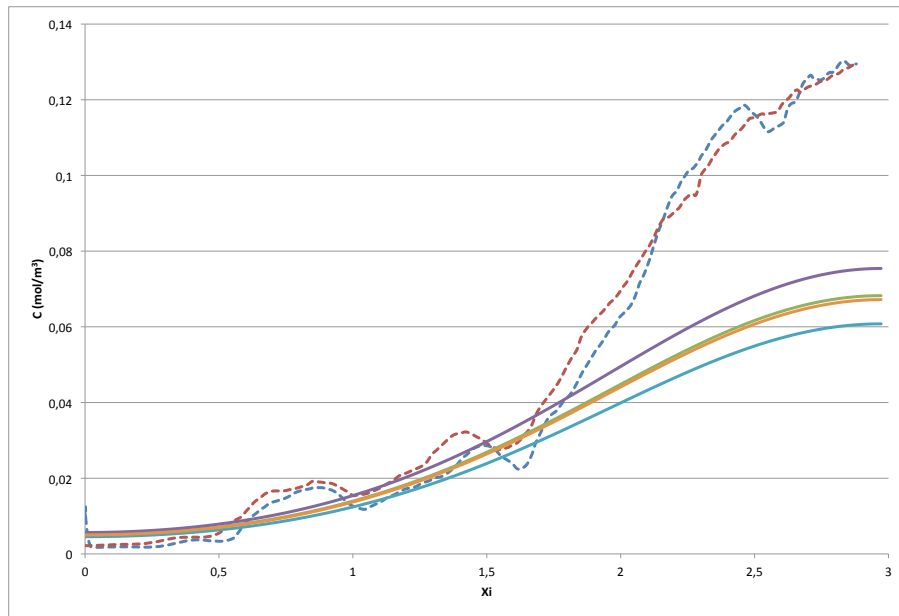


Figure 49: Concentration profiles for $N = 5.96$, $Re = 348$, correlation by Foumeny et al. at $z' = 10$

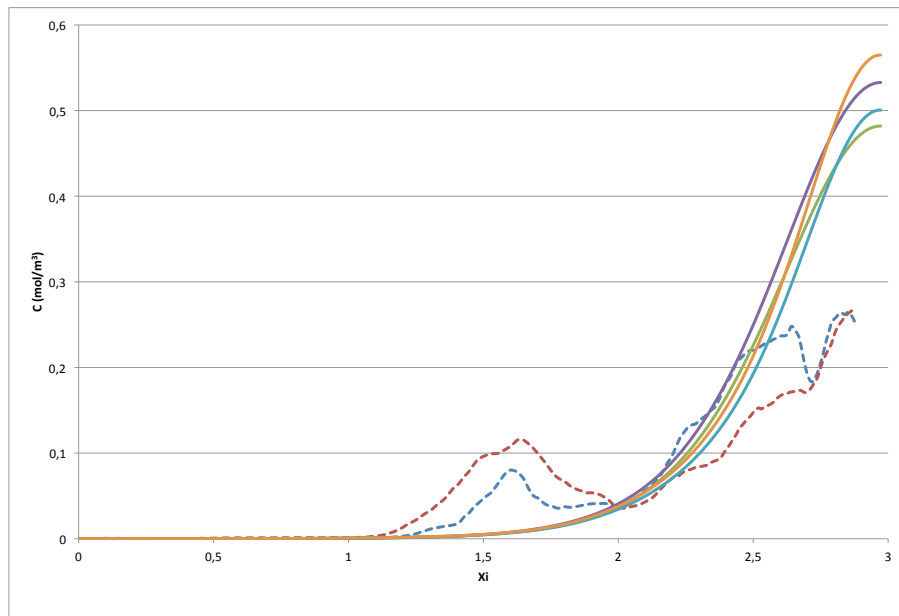


Figure 50: Concentration profiles for $N = 5.96$, $Re = 348$, correlation by Coelho et al. at $z' = 5$

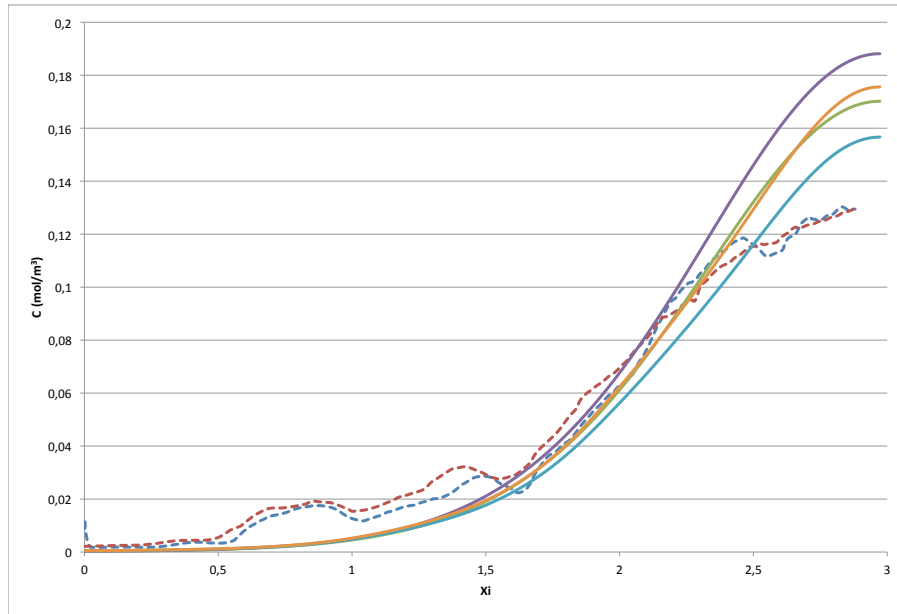


Figure 51: Concentration profiles for $N = 5.96$, $Re = 348$, correlation by Coelho et al. at $z'=10$

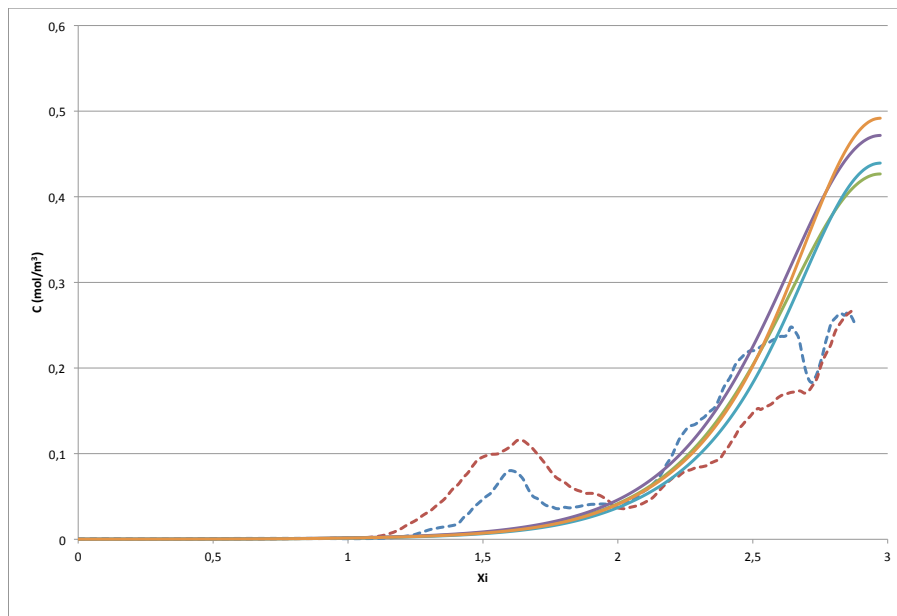


Figure 52: Concentration profiles for $N = 5.96$, $Re = 348$, correlation by Freund et al. at $z'=5$

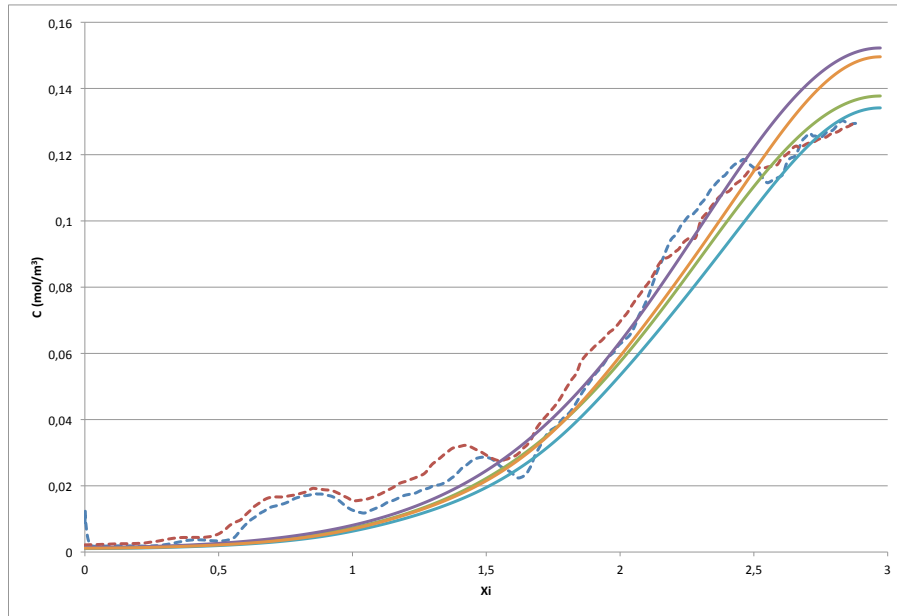


Figure 53: Concentration profiles for $N = 5.96$, $Re = 348$, correlation by Freund et al. at $z' = 10$

One can see the effect of the velocity profiles, as the axial dispersion is increased (concentration profiles lower at $z' = 10$) in all the cases when implementing the radial profiles, driving the reaction engineering calculations away from the CFD ones. The calculations based on Coelho et al. and Freund et al. correlations show a lower radial dispersion early in the tube when using the radial profiles. Indeed, the concentration profiles are higher in the center at $z' = 5$.

On another hand, the implementation of these profiles lead to almost no changes in the Peclet numbers. They both stay relatively unaltered along the Xi axis, as pictured on Figure 54 (Only the Foumeny et al. gaps configuration is showed). The values compare with the one obtained before implementation of the profiles.

These profiles were also obtained for other Reynolds, and the same conclusions can be drawn. Moreover, when reaching higher Reynolds numbers, the implementation of the radial profiles leads to less and less significant changes in the concentration profiles. When comparing the results for the Foumeny et al. correlation, the concentration profiles obtained with and without the radial dependence of the porosity and velocity were identical.

This lack of changes in the Peclet numbers explains the small changes in the

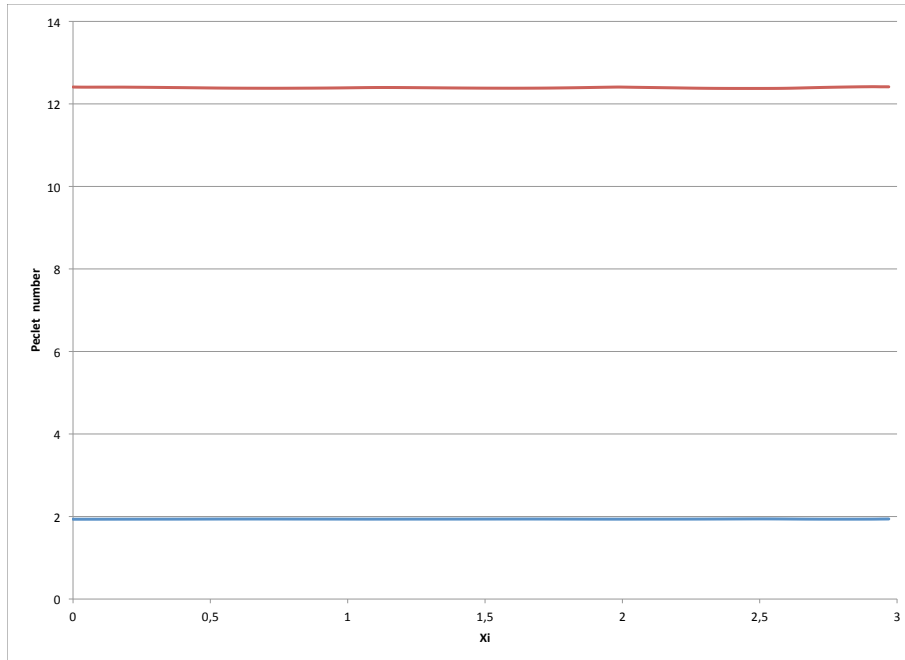


Figure 54: *Peclet numbers obtained in COMSOL for $N = 5.96$, $Re = 348$, gaps configuration, with porosity and interstitial velocity profiles*

profiles. A good improvement might be the implementation of a profile for the mean axial velocity instead of the mean velocity magnitude, which regroups both radial and axial, as an average, in the same calculation. The mean radial velocity could also be considered. However, obtaining such a profile would require a different method of extraction from the Fluent file than simply doing an average around the axis. Indeed, radial velocities from opposite sides of the axis of the tube would cancel each other when calculating the average.

2 Reaction models

We compare concentration profiles for both reactants and products at $z' = 5''$ and $z' = 10''$ from the inlet. We only used the correlation by Foumeny et al. to calculate the Peclet numbers in the reaction engineering model. The reaction being the principal factor of influence in the distribution of the species, the correlations that is used to not greatly influence the results. Moreover it seemed that the higher

the Reynolds, the closer the results from reaction engineering models were to CFD calculations when using the correlation by Foumeny et al., justifying its use. The reaction rate distribution is also compared.

Before starting the comparison, verifications were conducted on the Fluent file. First, the mass balance was checked, and an error of 1.6% was found between the inlet and $z' = 12$. Moreover, a problem arose when looking at the concentration profiles of H_2 . It seemed like H_2 was not reacting, with almost no evolution in the concentration along the z' axis. The reaction rate inside the particles was coherent, meaning that the production of H_2 was three times higher than the consumption of CH_4 . However, since we are supposed to be at steady state, the flux at the surface of the particle should equal the consumption inside this particle. This could be verified for all the species except H_2 .

Calculations were still conducted under COMSOL, and we compared the concentration profiles and outlet fluxes for CH_4 , CO and H_2O , as well as the reaction rates.

The validity of the COMSOL files was checked by evaluating the mass balances. The dimensionless reaction rate and outlet flowrate were compared for CH_4 , H_2 and CO . The mass fraction of H_2O being calculated as the complement of the others, we were not able to calculate its outlet flowrate or consumption rate. An error under 1% was considered acceptable. Table 11 gives the values and errors for each species for the mesh described in section III.2.

Model	species	Net flux	Consumption/production/transfer	Error (%)
P-H model	CH_4	0.1677	0.1676	0.6
	H_2	0.1128	0.1128	0.0
	CO	0.1313	0.1313	0.0
S-P model	CH_4	0.4796	0.4797	0.2
	H_2	0.1799	0.1799	0.0
	CO	0.8394	0.8394	0.0

Table 11: Comparison between net fluxes and consumption/production/transfer term in COMSOL. Dimensionless.

The volume integral calculated for the single pellet model is the transfer term implemented in the fluid equations. This term has to be compared to the flux at the surface of the particles and the reaction rate inside the particles. Table 12 compares the values of reaction rate and surface flux for the solid phase.

species	$\nu_i \Phi^2 \times rate$	Surface flux	Error (%)
CH_4	2606.79	2567.36	1.5
H_2	444.19	437.47	1.5
CO	6427.57	6330.35	1.5

Table 12: *Reaction rate and particle surface fluxes in COMSOL Single pellet model. Dimensionless.*

Finally, one must take into account the Sherwood and Stanton numbers when comparing the solid outlet flux and the transfer term of the fluid equations. In order to be compared, the dimensionless solid surface flux must be multiplied by St/Sh . This last comparison is given in Table 13.

species	Surface flux $\times St/Sh$	transfer term	Error (%)
CH_4	0.4741	0.4797	1.16
H_2	0.1778	0.1799	1.16
CO	0.8296	0.8394	1.16

Table 13: *Corrected solid surface flux and fluid transfer term.*

The next values that were checked are the values of the outlet fluxes. A comparison between the COMSOL and the Fluent model was done. As expected, the values are off, especially in the case of H_2 . Table 14 gives all the values calculated.

Specie	Fluent	COMSOL P-H		COMSOL S-P	
		Values	Error (%)	Values	Error (%)
CH_4	190.81	176.68	7.4	75.57	60.4
H_2	43.72	78.67	44.4	100.03	56.3
CO	180.44	156.12	13.47	383.62	53

Table 14: *Outlet fluxes (in $g.m^{-2}.s^{-1}$) for both models*

This last table clearly shows that there is a problem with the single pellet model. Indeed, the outlet fluxes of all species are off by at least 53%. This error is linked to the fact that in the model, as can be seen in equations 20 and 22, the porosity is not taken into account at all. This certainly leads to an over evaluation of the reaction, and therefore the high values of the fluxes for the products, and the low value for the reactant are understandable. Moreover, the high error in the evaluation of H_2 comes from the problem encountered in Fluent that we previously discussed.

$$\frac{-\partial C'_{f,i}}{\partial z'} + \frac{1}{Pe_{m,r,i}} \left(\frac{\partial^2 C'_{f,i}}{\partial r'^2} + \frac{1}{r'} \frac{\partial C'_{f,i}}{\partial r'} \right) + \frac{1}{Pe_{m,a,i}} \frac{\partial^2 C'_{f,i}}{\partial z'^2} = St_{m,i} (C'_{f,i} - C'^s_{s,i}) \quad (20)$$

$$\frac{-d^2 C'_{s,i}}{d\xi'^2} = \frac{2}{\xi'} \frac{dC'_{s,i}}{d\xi'} - \nu_i \Phi_i^2 \mathcal{R}(C'_{s,i}, T'_s) \quad (22)$$

After these verifications for the validity of the files, the concentration profiles in the fluid phase were plotted at $z = 7''$ and $z = 12''$. Figures 55 to 58 show the results for the pseudo-heterogeneous model. The red lines correspond to $z' = 7''$, the blue ones to $z' = 12''$. Dashed lines are for the fluent profiles, plain lines for the COMSOL model.

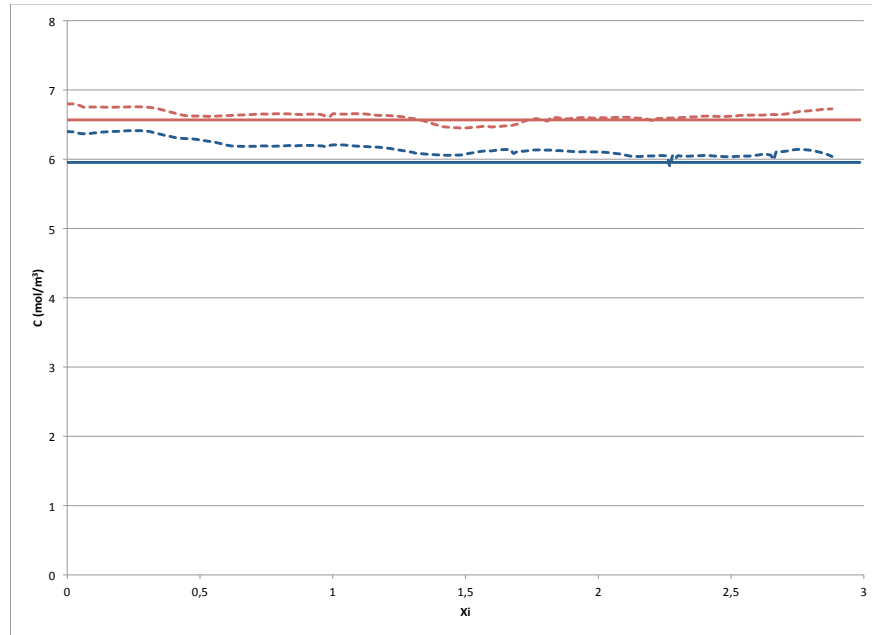


Figure 55: *Concentration profile of CH_4 at $z=7''$ and $12''$, Pseudo-heterogeneous model.*

One can clearly see the problem encountered with H_2 once again. It seems like H_2 is not reacting, staying at a concentration of approximately 11 mol.m^{-3} . The pseudo-heterogeneous model is able to predict the profiles of water and methane fairly accurately. There are no wall effects appearing, and the diffusion is definitely not dominant in this case, where the reaction rate controls the entire bed behavior

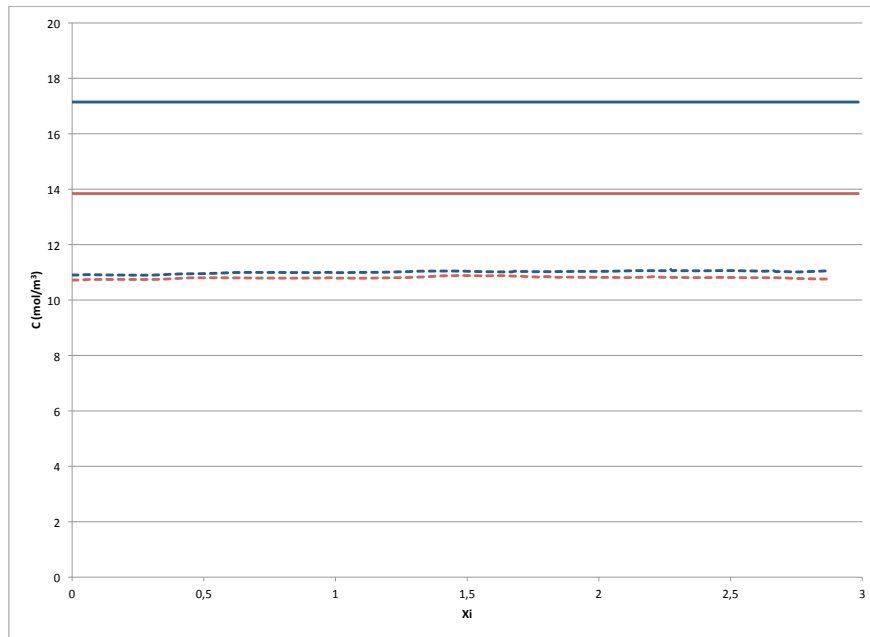


Figure 56: Concentration profile of H_2 at $z=7''$ and $12''$, Pseudo-heterogeneous model.

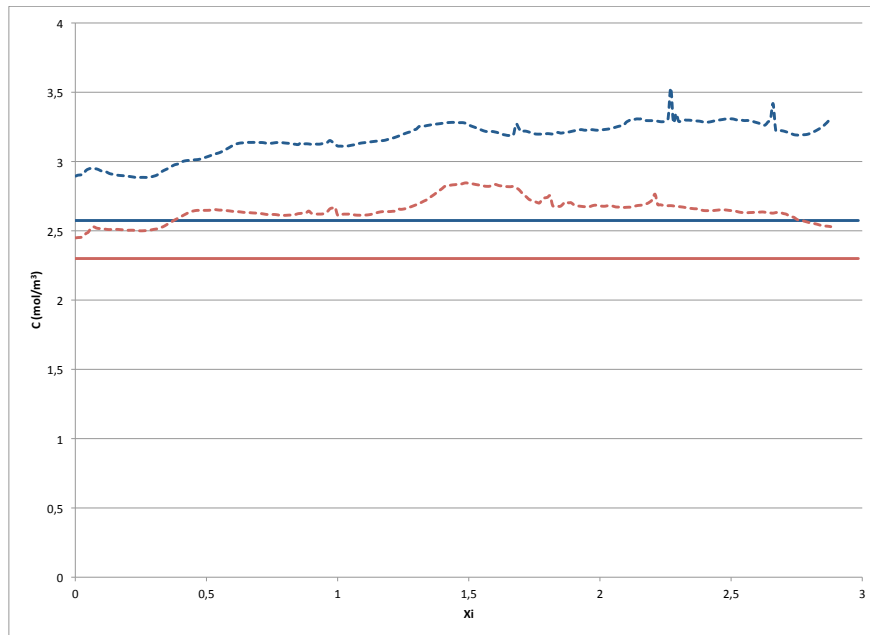


Figure 57: Concentration profile of CO at $z=7''$ and $12''$, Pseudo-heterogeneous model.

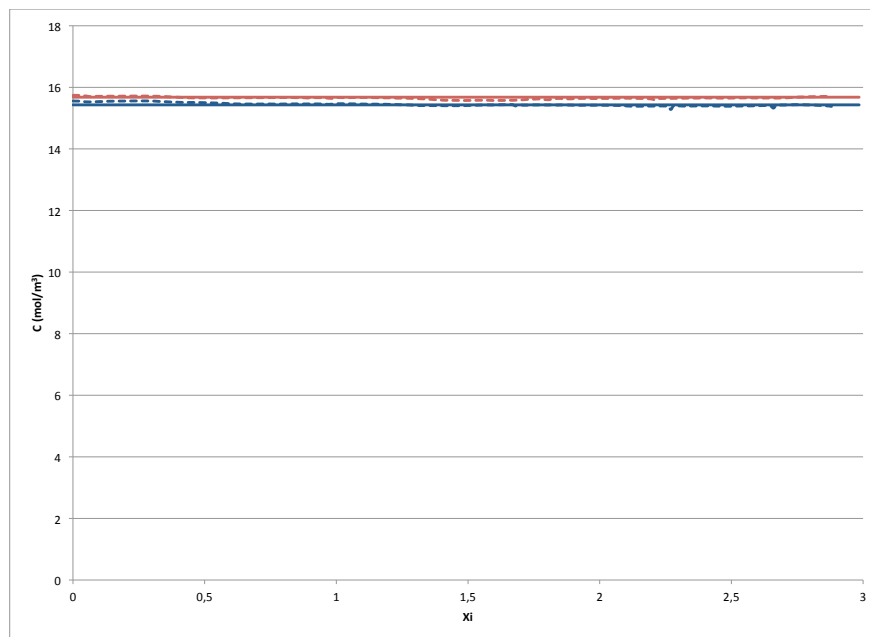


Figure 58: Concentration profile of H_2O at $z=7''$ and $12''$, Pseudo-heterogeneous model.

in term of concentration distribution. The wall effects could be introduced if a radial porosity profile was considered.

The fact that H_2 is not able to diffuse out of the particles in the fluent models shifts the reaction to the right. This can be seen as the production of CO being over estimated by the fluent model, and the consumption of methane being slightly under estimated. The order of magnitude however stays the same.

Figures 59 to 62 show the concentration profiles obtained with the single pellet model. Again, in red is $z' = 7''$, in blue $z' = 12''$. Dashed lines are for the fluent profiles, plain lines for the COMSOL model.

Clearly, this model is not consistent with the Fluent calculations. The reaction is over evaluated, as the products concentration are higher and the reactant lower than in Fluent. As explained before, this model does not take the porosity into account at all, which would explain this behavior. Therefore, the implementation of porosity is necessary in this model, especially for low N beds such as the one considered here.

An other problem that arise with this Single pellet model is that if the values of Sherwood and Stanton numbers are not selected carefully, the model will have

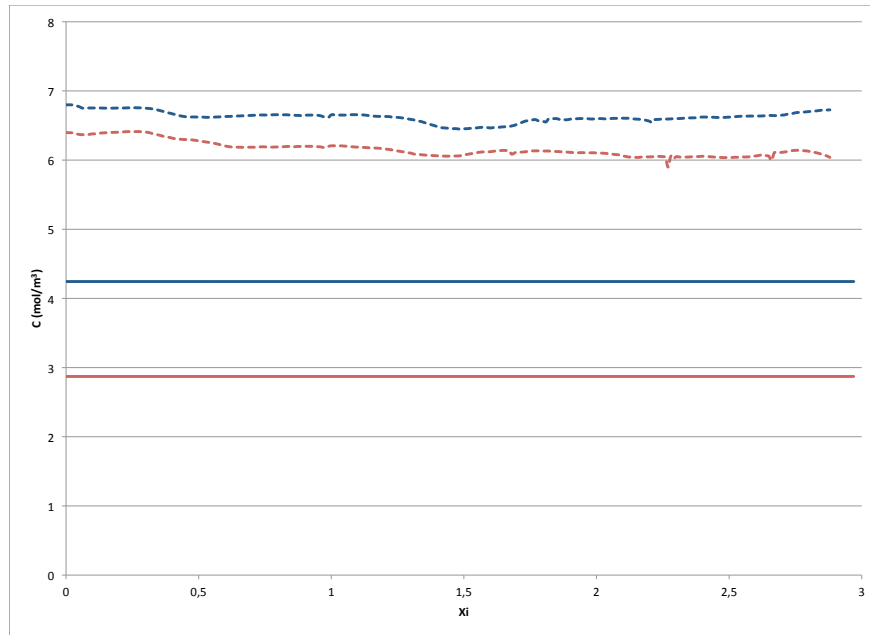


Figure 59: Concentration profile of CH_4 at $z=7''$ and $12''$, Single pellet model.

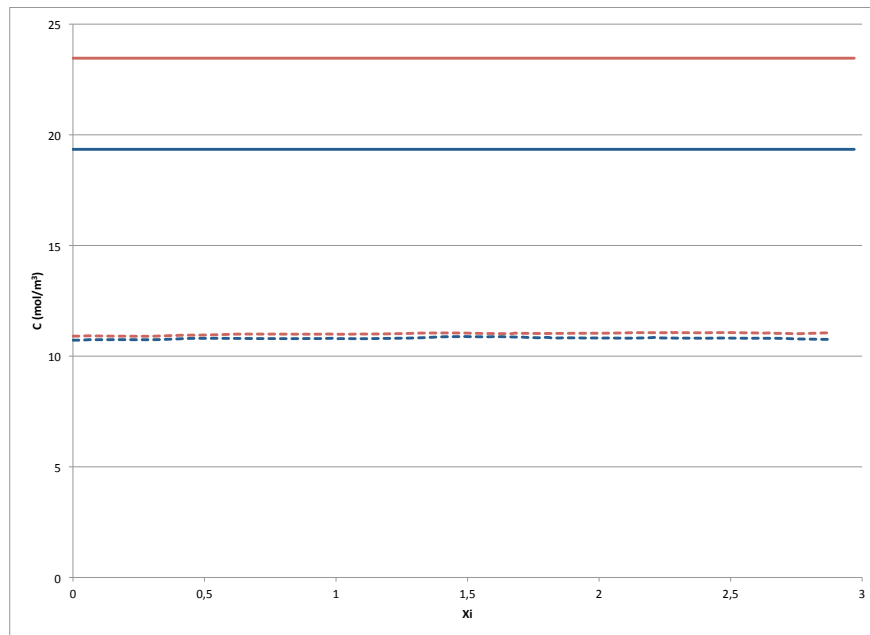


Figure 60: Concentration profile of H_2 at $z=7''$ and $12''$, Single pellet model.

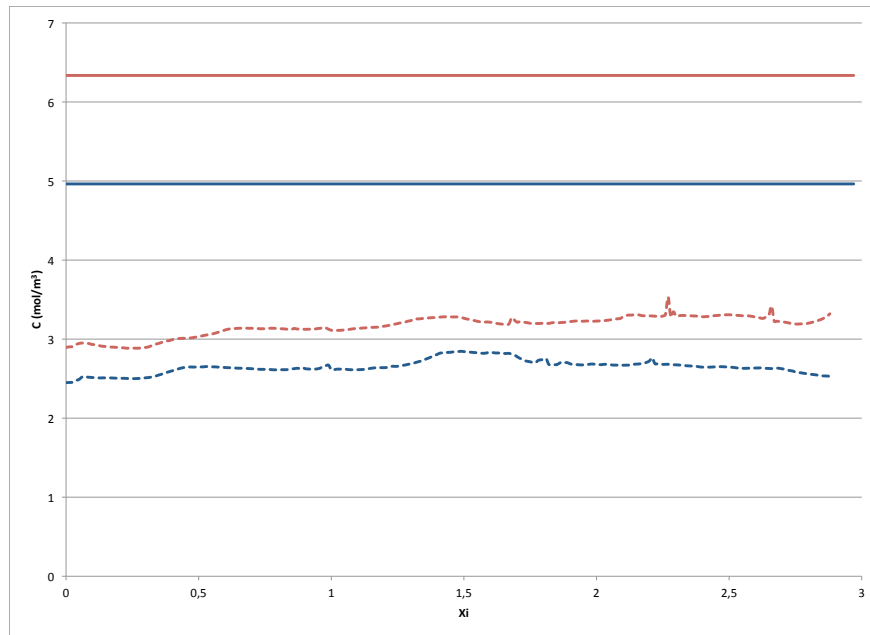


Figure 61: *Concentration profile of CO at $z=7''$ and $12''$, Single pellet model.*

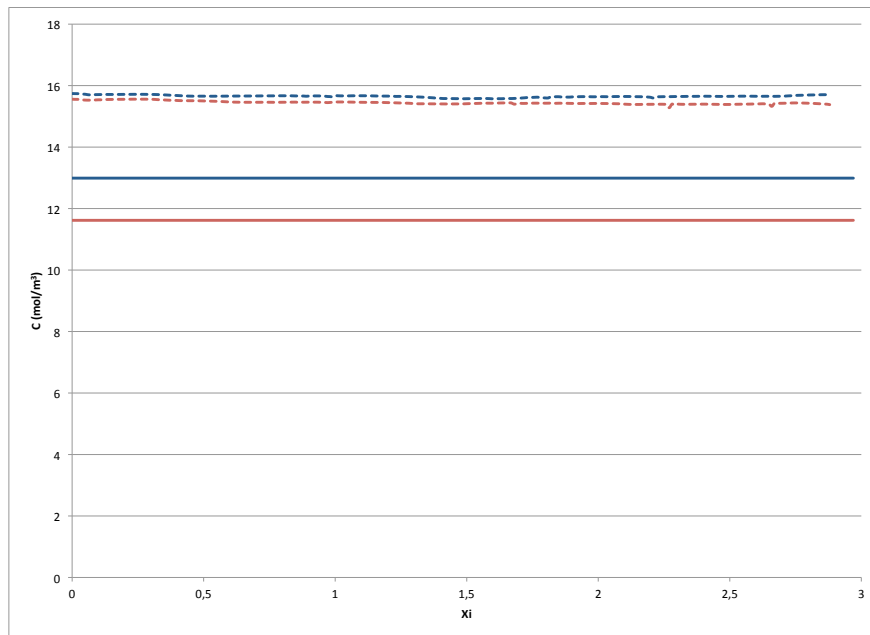


Figure 62: *Concentration profile of H₂O at $z=7''$ and $12''$, Single pellet model.*

problem at the interface between fluid and solid. Unfortunately it seems to be the case here, since the concentration differences between the fluid and solid surface reach values up to 2mol.m^{-3} in the case of H_2 , which is relatively high. This problem needs to be carefully considered, and the mass transfer coefficients between the solid and the fluid might have to be revised.

One way to first check these parameters would be to evaluate the fluxes between fluid and solid in Fluent and compare them to the COMSOL ones. This would give a first idea of the parameters that could need improvement.

Conclusion

This study was developed as an evaluation of the classical reaction engineering to predict the behavior of two low bed-to-particle diameter ratio beds. Two aspects were studied, the mass dispersion of a species in a bed of non porous particles, and the dispersion of species in a bed where the particles are implemented with a reaction of methane conversion.

The first part of the analysis, the evaluation of dispersion, gave satisfactory results, as the dispersion models fitted the computational fluid dynamics calculations. In the case of $N = 5.96$, the correlations that were studied did not give perfect results, but the overall shape and behavior of the bed simulated with the dispersion models on COMSOL were close to the one observed in Fluent. For the $N = 7.99$ bed, the results were satisfactory, and the correlations proposed by Foumeny et al. lead to values of Peclet numbers that were able to successfully predict the behavior of the bed, for several Reynolds numbers.

We then looked at a low N tube with an isothermal reaction. We encountered a problem of convergence with the CFD calculations, as one of the species involved in the reaction did not reach steady state. We looked into this problem of convergence under several angles, but no solution was found in time. Comparison between CFD calculations and two reaction engineering models were still done. It seems that a pseudo-heterogeneous model is fairly able to simulate the reaction inside such a tube, using the Foumeny et al. correlations for Peclet number, given the fact that the Reynolds number is high enough. The reaction seems to be the main phenomenon responsible for the concentration changes in the bed, and therefore, the dispersion part of the problem is not important enough to disturb the results. The second model, the single pellet model, did not live up to our expectations, mainly because it requires a high precision in the choice of the parameters that govern mass transfer between the two phases. Moreover, it does not include porosity at any level, therefore over evaluating the reaction.

Recommendation

1 Dispersion calculations

In order to validate the results obtained here regarding dispersion, one should try to obtain average concentration profiles, using different beds, and different positions in these beds.

Obtaining averages for the velocity profiles using these different beds could also help understand how to implement these profile in a better way in the reaction engineering models. Moreover, obtaining profiles not only depending on the radial coordinate, but also on the axial one might be beneficial. This would, however, require a longer bed.

Calculations should also be run for lower N , such as 3.96.

Heat dispersion now needs to be evaluated, through the same kind of assessment than for mass transfer.

2 Reaction calculations

The problem in the Fluent file needs to be solved. One could look into a better diffusivity for hydrogen, or a way to accelerate convergence. Starting the calculations with a higher hydrogen mass fraction in the particles might be a good option.

The single pellet model coefficient need to be revised, particularly the Stanton and Sherwood numbers. Moreover, the implementation of a porosity and velocity profile could lead to some improvement in the overall prediction of the concentration profiles and reaction rate.

Calculations including a non iso-thermal tube need to be done as well, in order to evaluate the models globally, when computing simultaneously mass and heat transfer phenomena.

Nomenclature

Bi_s	Biot number for the fluid-particle interface, $\frac{h_s d_p}{\lambda}$
Bi_w	Biot number for the fluid-wall interface, $\frac{h_w d_p}{\lambda}$
C	Concentration $mol.m^{-3}$
C'	Reduced concentration $\frac{C}{C_{in}}$
C_{in}	Total inlet concentration $mol.m^{-3}$
$C_{p,f}$	Fluid heat capacity, $J.mol^{-1}.K^{-1}$
C_{tot}	Fluid total concentration, $mol.m^{-3}$
D_a	Axial component of the diffusivity, $m^2.s^{-1}$
D_e	Diffusivity inside the catalyst particle, $m^2.s^{-1}$
D_m	Molecular diffusivity, $m^2.s^{-1}$
D_r	Radial component of the diffusivity, $m^2.s^{-1}$
Da	Damkhöler number, $\frac{\rho d_p R(C_{i,in}, T_{in})}{u C_{tot}}$
Da_i	Damkhöler number for calculations based on mass fractions, $\frac{\rho d_p R(C_{i,in}, T_{in}) M_i}{u \rho_f}$
d_p	Catalyst Particle diameter, m
d_t	Bed diameter, m
ΔH	Enthalpy of reaction $J.mol^{-1}$
h_s	Fluid to solid heat transfer coefficient, $W.m^{-2}$
h_w	Fluid to wall heat transfer coefficient, $W.m^{-2}$
k_g	Fluid to solid mass transfer coefficient, $m.s^{-1}$
k_r	Reaction rate constant, $mol.kg_{cat}^{-1}.s^{-1}$
k_s	Solid thermal conductivity $W.K^{-1}.m^{-1}$
N	Aspect ratio of the bed, $\frac{d_t}{d_p}$
$Pe_{h,a}$	Axial heat Peclet number, $\frac{u_o \rho_f C_{p,f} d_p}{k_{a,eff}}$
$Pe_{h,r}$	Radial heat Peclet number, $\frac{u_o \rho_f C_{p,f} d_p}{k_{r,eff}}$
Pe_m	Molecular mass Peclet number, $\frac{u_o d_p}{D_m}$

$Pe_{m,a}$	Axial mass Peclet number, $\frac{u_0 d_p}{D_a}$
$Pe_{m,r}$	Radial mass Peclet number, $\frac{u_0 d_p}{D_r}$
r	Bed radial coordinate m
r'	Reduced bed radial coordinate $\frac{r}{d_p}$
R	Ideal gas constant, $kJ.mol^{-1}.K^{-1}$
$R(C_i, T)$	Reaction rate, $mol.kg_{cat}^{-1}.s^{-1}$
$\mathcal{R}(C_i, T)$	Reduced reaction rate, $\frac{R(C_i, T)}{R(C_{i,in}, T_{in})}$
Re_0	Reynolds number based on superficial velocity, $\frac{u_0 d_p}{\nu}$
Re	Reynold number based on interstitial velocity, $\frac{u d_p}{\nu}$
Sc	Schmidt number, $\frac{\nu}{D_m}$
Sh_i	Sherwood number for the solid, $\frac{k_{g,i} d_p}{D_{e,i}}$
St_h	Heat Stanton number, $\frac{a_p h d_p}{u_0 \rho_f C_{p,f}}$
St_m	Mass Stanton number, $\frac{a_p k_{g,i} d_p}{u_0}$
T	Temperature K
T'	Reduced temperature $\frac{T}{T_{in}}$
T_{in}	Inlet temperature of the fluid, K
u	Interstitial velocity, $= u_0 \epsilon$, $m.s^{-1}$
u_0	Superficial velocity, $m.s^{-1}$
z	Bed axial coordinate, m
z'	Bed reduced axial coordinate, $\frac{z}{d_p}$
Greek Letters:	
β_f	Adiabatic temperature rise of the fluid, $\frac{(-\Delta H)C_{tot}}{\rho_f C_{p,f} T_{in}}$
$\beta_{s,i}$	Adiabatic temperature rise in the solid particle, $\frac{(-\Delta H)C_{s,i} D_{e,i}}{k_s T_{in}}$
ϵ	Bed porosity
η	Effectiveness factor for species i .
ρ	Density, $kg.m^{-3}$

λ	Thermal conductivity of the fluid, $W.m^{-1}.K^{-1}$
ν	Dynamic viscosity, $m^2.s^{-1}$
ν	Stoichiometric coefficient
τ	Bed tortuosity
Φ	Thiele Modulus, $\left(\frac{d_p \rho_s R(C_{s,i}, T)}{D_{e,i} C_{s,i} / d_p}\right)^{1/2}$
Subscript	
f	Refers to the fluid phase
s	Refers to the solid phase
w	Refers to the tube wall
i	Refers to species i

References

- [1] B. AHN AND A. ZOULALIAN, *Axial dispersion in packed beds with large wall effects*, *AIChE Journal*, 32 (1986), pp. 170–174.
- [2] T. ATMAKIDIS AND E. KENIG, *CFD-based analysis of the wall effect on the pressure drop in packed beds with moderate tube/particle diameter ratios in the laminar flow regime*, *Chemical Engineering Journal*, 155 (2009), pp. 404–410.
- [3] F. AUGIER, F. IDOUX, AND J. DELENNE, *Numerical simulations of transfer and transport properties inside packed beds of spherical particles*, *Chemical Engineering Science*, 65 (2010), pp. 1055–1064.
- [4] D. COELHO, J.-F. THOVERT, AND P. ADLER, *Geometrical and transport properties of random packings of spheres and aspherical particles*, *Physical review E*, 55 (1997), pp. 1959–1978.
- [5] J. G. DE CARVALHO AND J. DELGADO, *Overall map and correlation of dispersion data for flow through granular packed beds*, *Chemical Engineering Science*, 60 (2005), pp. 365–375.
- [6] J. DELGADO, *A critical review of dispersion in packed beds*, *Heat and Mass Transfer*, 42 (2006), pp. 279–310.
- [7] A. DIXON, M. DICOSTANZO, AND B. SOUCY, *Fluid-phase radial transport in packed beds of low tube-to-particle diameter ratio*, *Int. J. Heat and Mass Transfer*, 27 (1984), pp. 1701–1713.
- [8] R. FAHIEN AND J. SMITH, *Mass transfer in packed beds*, *AIChE Journal*, 1 (1955), pp. 28–37.
- [9] E. FOUMENY, M. CHOWDHURY, C. MCGREAVY, AND J. CASTRO, *Estimation of dispersion coefficients in packed beds*, *Chemical Engineering Technology*, 15 (1992), pp. 168–181.
- [10] H. FREUND, J. BAUER, T. ZEISER, AND G. EMIG, *Detailed simulation of transport processes in fixed-beds*, *Industrial and Engineering Chemistry Research*, 44 (2005), pp. 6423–6434.
- [11] G. FROMENT AND H. HOFMANN, *Design of fixed-bed gas-solid catalytic reactors*, in *Chemical Reaction and Reactor Engineering*, J. Carberry and A. Varma, eds., American Chemical Society, 1987, pp. 373–440.

- [12] D. GUNN, *Axial and radial dispersion in fixed beds*, Chemical Engineering Science, 42 (1987), pp. 363–373.
- [13] J. HIBY, *Longitudinal and transverse mixing during single-phase flow through granular beds*, Interaction between fluids and particles (London: Instn chem. engrs), (1962), pp. 312–325.
- [14] K. HOU AND R. HUGHES, *The kinetics of methane steam reforming over a Ni/α – Al₂O catalyst*, Chemical Engineering Journal, 82 (2001), pp. 311–328.
- [15] M. KUROKI, S. OOKAWARA, D. STREET, K. OGAWAA, *High-fidelity CFD modeling of particle-to-fluid heat transfer in packed bed reactors*, Copenhagen, September 2007, European Congress of Chemical Engineering.
- [16] P. MAGNICO, *Hydrodynamic and transport properties of packed beds in small tube-to-sphere diameter ratio: pore scale simulation using an eulerian and a langrangian approach*, Chemical Engineering Science, 58 (2003), pp. 5005–5024.
- [17] N. MARIANI, O. MARTINEZ, AND G. BARRETO, *Computing radial packing properties from the distribution of particle centers*, Chemical Engineering Science, 56 (2001), pp. 5693–5707.
- [18] G. MUELLER, *Numerically packing spheres in cylinders*, Powder Technology, 159 (2005), pp. 105–110.
- [19] M. NIJEMEISLAND AND A. DIXON, *Comparison of CFD simulations to experiment for convective heat transfer in a gas-solid fixed bed*, Chemical Engineering Journal, 82 (2001), pp. 231–146.
- [20] W. SALVAT, N. MARIANI, G. BARRETO, AND O. M. INEZ, *An algorithm to simulate packing structure in cylindrical containers*, Catalysis Today, 107-108 (2005), pp. 513–519.
- [21] K. SCHNITZLEIN, *Modelling radial dispersion in terms of the local structure of packed beds*, Chemical Engineering Science, 56 (2001), pp. 579–585.
- [22] D. SCOTT, W. LEE, AND J. PAPA, *The measurement of transport coefficients in gas-solid heterogeneous reactions*, Chemical Engineering Science, 29 (1974), pp. 2155–2167.
- [23] D. TANG, A. JESS, X. REN, B. BLUEMICH, AND S. STAPF, *Axial dispersion and wall effects in narrow fixed bed reactors: a comparative study based on RTD*

- and NMR measurements*, Chemical Engineering Technology, 27 (2004), pp. 866–873.
- [24] J. URBAN AND A. GOMEZPLATA, *Axial dispersion coefficients in packed beds at low reynolds numbers*, Canadian Journal of Chemical Engineering, 47 (1969), pp. 353–359.
- [25] D. ZIOLKOWSKI AND S. SZUSTEK, *Effect of fluid velocity radial profile on the radial mass dispersion in a fluid stream in a packed bed tubular apparatus*, Chemical Engineering Science, 44 (1989), pp. 1195–1204.

Appendices

A Reaction Parameters

All these reaction parameters are extracted from the literature [14].



$$r = \frac{k_1(P_{CH_4}P_{H_2O}^{0.5}/P_{H_2}^{1.25})(1 - (P_{CO}P_{H_2}^3/K_{p1}P_{CH_4}P_{H_2O}))}{den^2}$$

whith

$$den = 1 + K_{CO}P_{CO} + K_H P_H^{0.5} + K_{H_2O}(P_{H_2O}/P_{H_2})$$

These parameters are determined using the van't Hoff and Arrhenius equations:

$$k_1 = A_1 \exp\left(-\frac{E_1}{RT}\right)$$

$$K_i = A(K_i) \exp\left(\frac{-\Delta H_{i,a}}{RT}\right)$$

The following table gives the values of each constant.

Parameter	Value
A_1 ($kmol/kg_{cat}.s.kPa^{0.25}$)	5.922×10^8
E_1 ($kJ.mol^{-1}$)	209.2
$A(K_{CO})$ (kPa^{-1})	5.127×10^{-13}
$\Delta H_{CO,a}$ (kJ/mol)	-140.0
$A(K_H)$ ($kPa^{-0.5}$)	5.68×10^{-10}
$\Delta H_{H,a}$ (kJ/mol)	-93.4
$A(K_{H_2O})$	9.251
$\Delta H_{H_2O,a}$ (kJ/mol)	15.9

Table 16: Values of the constants required for the calculation of the reaction rate

Also, we have $K_{p1} = 1.198 \times 10^{17} \exp(-26830/T)$ (kPa^2)

B Values of axial and radial Peclet numbers for the different correlations

B.1 Foumeny et al.

$$\frac{1}{Pe_{m,r}} = \frac{0.34}{(Re_0Sc)^{0.80}} + \frac{0.08}{\left(1 + \frac{10.8}{Re_0Sc}\right)}$$

$$\frac{1}{Pe_{m,a}} = \frac{0.72}{ReSc} + \frac{0.52}{\left(1 + \frac{9.0}{ReSc}\right)}$$

u ($m.s^{-1}$)	0.05	0.2	0.4	0.5
$Pe_{m,r}$	12.393	12.383	12.406	12.414
$Pe_{m,a}$	2.003	1.943	1.933	1.931

Table 17: Values of Peclet numbers calculated with the correlation from Foumeny et al.

B.2 Coelho et al.

$$\frac{D_{rad}}{\mathcal{D}_m} = 0.164Pe_m^{0.72}$$

$$\frac{D_{ax}}{\mathcal{D}_m} = 0.106Pe_m^{1.29}$$

u ($m.s^{-1}$)	0.05	0.2	0.4	0.5
$Pe_{m,r}$	20.752	30.595	37.148	39.543
$Pe_{m,a}$	2.653	1.775	1.452	1.361

Table 18: Values of Peclet numbers calculated with the correlation from Coelho et al.

B.3 Freud et al.

$$\frac{D_{rad}}{\mathcal{D}_m} = \frac{1}{\tau} + \frac{Pe_m^{\alpha_{rad}}}{\beta_{rad}}$$

$$\frac{D_{ax}}{\mathcal{D}_m} = \frac{1}{\tau} + a_1 Pe_m + a_2 Pe_m \ln(Pe_m)$$

$u \text{ (} m.s^{-1} \text{)}$	0.05	0.2	0.4	0.5
$Pe_{m,r}$	16.509	22.565	25.596	26.595
$Pe_{m,a}$	1.269	0.974	0.871	0.842

Table 19: Values of Peclet numbers calculated with the correlation from Freud et al.